Eur. Phys. J. C (2023) 83:661
https://doi.org/10.1140/epjc/s10052-023-11729-y

THE EUROPEAN PHYSICAL JOURNAL C

Regular Article - Experimental Physics

Inclusive photon production at forward rapidities in pp and p–Pb collisions at $\sqrt{s_{\mathrm{NN}}} = 5.02$ TeV

ALICE Collaboration[*]

CERN, 1211 Geneva 23, Switzerland

Received: 21 March 2023 / Accepted: 18 June 2023 / Published online: 25 July 2023

Abstract A study of multiplicity and pseudorapidity distributions of inclusive photons measured in pp and p–Pb collisions at a center-of-mass energy per nucleon–nucleon collision of $\sqrt{s_{\mathrm{NN}}} = 5.02$ TeV using the ALICE detector in the forward pseudorapidity region $2.3 < \eta_{\mathrm{lab}} < 3.9$ is presented. Measurements in p–Pb collisions are reported for two beam configurations in which the directions of the proton and lead ion beam were reversed. The pseudorapidity distributions in p–Pb collisions are obtained for seven centrality classes which are defined based on different event activity estimators, i.e., the charged-particle multiplicity measured at midrapidity as well as the energy deposited in a calorimeter at beam rapidity. The inclusive photon multiplicity distributions for both pp and p–Pb collisions are described by double negative binomial distributions. The pseudorapidity distributions of inclusive photons are compared to those of charged particles at midrapidity in pp collisions and for different centrality classes in p–Pb collisions. The results are compared to predictions from various Monte Carlo event generators. None of the generators considered in this paper reproduces the inclusive photon multiplicity distributions in the reported multiplicity range. The pseudorapidity distributions are, however, better described by the same generators.

1 Introduction

The primary goal of high-energy heavy-ion physics is the study of a new state of nuclear matter, the quark–gluon plasma (QGP), a thermalized system of partons (quarks and gluons) [1–3]. The study of proton–proton (pp) and proton–nucleus (p–A) collisions provides the baseline for the interpretation of the effects of the QGP formation that are observed in heavy-ion collisions. In addition, the study of p–A collisions helps to understand the effects of cold nuclear matter on the production of final-state particles. Among these effects, an important role is played by transverse momentum (k_{T}) broadening of initial- and final-state partons [4], and by the modification of the parton distributions functions in bound nucleons compared to those of free nucleons, leading in particular to a reduction of parton densities (shadowing) at small parton fractional momentum x [5]. Interestingly, recent experimental results in pp and p–A collisions particularly at high multiplicities have shown features such as collective flow and strangeness enhancement which are usually attributed to the formation of a QGP in heavy-ion collisions [6–13]. The origin of these phenomena in pp and p–A systems is not yet fully understood and under active scrutiny by the community. It is therefore important to understand the global properties of the system produced in pp and p–A collisions. Multiplicity and pseudorapidity distributions of produced particles are some examples of global observables, providing important information about the particle production mechanisms in these collisions. The integrated yield of particle production is mostly dominated by soft quantum chromodynamics (QCD) interactions, i.e. small momentum transfer (Q^2) processes, and is described by non-perturbative phenomenological models. On the other hand, the hard particle production (large Q^2) can be described by the well-established theory of perturbative quantum chromodynamics (pQCD). Measurements of multiplicity and pseudorapidity distributions provide important constraints on these models. Moreover, the variation of pseudorapidity (η) density of produced particles ($\mathrm{d}N/\mathrm{d}\eta$) with collision centrality can be parametrized by using a two-component model to extract the relative contributions to particle production from hard scatterings and soft processes [14,15].

The measurement of the multiplicity of inclusive photons provides complementary information with respect to those of charged particles as the inclusive photons are mostly produced in the decay of neutral pions (π^0) [16–18]. A comparative study of charged particles and inclusive photons can shed light on the possible similarities and/or differences in the underlying mechanisms of charged and neutral particle production.

At the Large Hadron Collider (LHC) energies, the underlying mechanisms of particle production could be different

[*] e-mail: alice-publications@cern.ch

at central and forward rapidities. Charged-particle multiplicity measurements at the LHC were previously performed by ALICE, ATLAS, CMS, and LHCb experiments in pp, p–Pb, and Pb–Pb collisions [19–43]. Inclusive photon production at forward rapidity was studied in pp collisions at $\sqrt{s} = 0.9$, 2.76, and 7 TeV by ALICE [16]. At midrapidity, the mean charged-particle multiplicity is found to follow a power law dependence on $\sqrt{s}$ [20–22] whereas the mean multiplicity of inclusive photons at forward rapidity can be described by both a logarithmic and a power law dependence with $\sqrt{s}$ at LHC energies [16].

In the present study, measurements of multiplicity and pseudorapidity distributions of inclusive photons at forward rapidity are reported for pp, p–Pb, and Pb–p collisions at $\sqrt{s_{\rm NN}} = 5.02$ TeV with ALICE. The dependence of the inclusive photon production on the centrality of the collision, which is related to the impact parameter of the p–A collision, and its scaling behavior with the number of participating nucleons ($N_{\rm part}$) at forward rapidity is also studied for the first time in p–Pb collisions at $\sqrt{s_{\rm NN}} = 5.02$ TeV. This measurement enables an extension of our understanding of particle production at forward rapidity.

This paper is organized as follows. The ALICE subdetectors relevant for the measurement of inclusive photons are described in Sect. 2. The data samples used in this analysis and the selection of events are discussed in Sect. 3. Section 4 discusses the details of the used centrality estimators. A discussion on Monte Carlo (MC) event generators and the simulation framework is given in Sect. 5. The reconstruction of inclusive photons is presented in Sect. 6. The correction for instrumental effects using the unfolding method is described in Sect. 7. Section 8 discusses the estimation of systematic uncertainties from various sources. Section 9 presents the results of inclusive photon multiplicity and pseudorapidity distributions obtained in this analysis and the outcome of this study is summarized in Sect. 10.

2 Experimental setup

A comprehensive description of the ALICE detectors and their performances can be found in Refs. [44,45]. The photon multiplicity detector (PMD) is used for the detection of inclusive photons at forward rapidity whereas for the purpose of event selection and centrality determination, the Silicon Pixel Detector (SPD), the V0 detector and the Zero Degree Calorimeter (ZDC) are used in this analysis. The ALICE reference frame is defined with the z axis directed along the beam line, the nominal interaction point (IP) at $z = 0$, and the positive z direction pointing towards the PMD.

The PMD is a preshower detector to measure inclusive photon multiplicity and its spatial distribution in the forward rapidity region. It is a gaseous detector placed at $z = 367$ cm covering the pseudorapidity region of $2.3 < \eta_{\rm lab} < 3.9$ with full azimuth coverage. The PMD consists of two fine granular planes: the charged particle veto plane and the preshower (PRE) plane. A lead converter with a thickness of three radiation lengths ($3X_0$) is placed between these two planes. The PMD consists of 184,320 hexagonal cells of size 0.22 cm^2 and depth of 0.5 cm with a copper honey-comb shaped cathode extended towards a 20 μm thick gold-plated tungsten wire at ground potential at the center of each cell. The cells are arranged in 40 modules in two planes. Each cell is filled with a gas mixture of Ar and CO_2 with a 70:30 ratio. Due to the presence of the lead converter, the incident photons produce electromagnetic showers by pair production and bremsstrahlung radiation and hit several cells in the PRE plane. On the other hand, charged hadrons generally fire only one or two cells in the PRE plane and produce a signal typical of a minimum ionizing particle. After receiving signals in the PRE plane a photon reconstruction algorithm is applied and a photon-rich sample of clusters is obtained by applying suitable rejection criteria to remove clusters from hadrons and from secondary particles as discussed in Sect. 6. The performance of the PMD is described in Refs. [16,46,47].

The SPD makes up the two innermost cylindrical layers of the ALICE Inner Tracking System (ITS) [48] surrounding the beam pipe. The two layers cover the pseudorapidity ranges $|\eta_{\rm lab}| < 2$ (inner layer) and $|\eta_{\rm lab}| < 1.4$ (outer layer). For this analysis, the SPD is mainly used in the determination of the position of the interaction vertex, the selection of the minimum bias (MB) trigger (combined with V0), and the centrality estimation [25–27]. The V0 detector [49,50] is made of two scintillator arrays placed on either side of the IP at $z = 330$ cm (V0A, covering the pseudorapidity interval $2.8 < \eta_{\rm lab} < 5.1$), and $z = -90$ cm (V0C, covering $-3.7 < \eta_{\rm lab} < -1.7$). The V0 is used for event selection and the determination of collision centrality [25,26,29,32]. The ZDC [51] consists of two sets of neutron (ZNA and ZNC) and proton (ZPA and ZPC) calorimeters positioned at $\pm$ 112.5 m from the IP, on both sides. The ZPA and ZPC calorimeters cover the pseudorapidity range $6.5 < |\eta_{\rm lab}| < 7.4$, while the ZNA and ZNC calorimeters have a geometric coverage $|\eta_{\rm lab}| > 8.8$. The energy detected by the ZN calorimeter on the Pb-remnant side (ZNA) is used to determine the centrality in p–Pb collisions [25,26].

3 Data sample and event selection

The p–Pb and pp data samples used in this analysis were collected in 2013 during LHC Run 1 and in 2015 during LHC Run 2, respectively. The p–Pb collisions were recorded for two beam configurations: in one (denoted as p–Pb), the proton beam at 4 TeV energy was pointing towards the negative z direction in the ALICE reference system [52], while the lead

ions at 1.58 TeV per nucleon energy moved in the opposite direction; in the other configuration (denoted as Pb–p), the directions of both proton and lead ion beams were reversed. The nucleon–nucleon center-of-mass energy for both configurations resulted in $\sqrt{s_{\rm NN}} = 5.02$ TeV. Due to the asymmetry of the beam energies, the nucleon–nucleon center-of-mass system in p–Pb collisions is shifted in rapidity by $\Delta y = 0.465$ with respect to symmetric pp collisions in the direction of the proton beam. In the following, the variable $\eta_{\rm lab}$ is used to indicate the pseudorapidity in the laboratory reference frame. For pp collisions, the center-of-mass frame is same as the laboratory frame.

In pp collisions, a sample of inelastic (INEL) events was selected using a MB trigger condition, which required the detection of at least one particle in either of the two V0 scintillator arrays or in the SPD. For p–Pb and Pb–p data samples, non-single diffractive (NSD) events were selected using a MB trigger condition, which required signals in both V0A and V0C (V0-AND requirement). The background events such as beam–gas or beam–halo interactions occurring outside the interaction region were rejected using the timing information from the V0 detector. Pile-up events, in which two or more collisions are detected as single events, were minimized using the procedure outlined in Ref. [22]. Events were further selected by restricting the reconstructed primary vertex position along the beam axis within $\pm$ 10 cm from the nominal IP. After applying all selection criteria, about 23 M INEL pp collisions, 90 M NSD p–Pb events, and 1.2 M NSD Pb–p collisions are considered for this analysis.

4 Centrality determination in p–Pb collisions

In p–Pb collisions, the centrality is determined using two centrality estimators. The first is based on the number of clusters in the outer layer of the SPD (CL1) at midrapidity and the second one makes use of the energy deposited in the neutron calorimeter in the Pb-remnant side at large rapidity (ZNA for the p–Pb beam configuration). Multiplicity-based centrality selection is performed by fitting the multiplicity distribution of the number of SPD clusters with a Glauber MC model [53,54] combined with a simple model for particle production, which assumes that the multiplicity at midrapidity has an average value proportional to $N_{\rm part}$ and a probability distribution described by a negative binomial distribution (NBD). Details about this method can be found in Ref. [25]. However, in p–Pb collisions, multiplicity fluctuations have a large influence on the centrality determination compared to the same effect in heavy-ion collisions as these fluctuations are sizable compared to the width of the $N_{\rm part}$ distribution. Other effects, originating, e.g., from the fragmentation of partons produced in hard scatterings, were found to bias the estimation of the centrality based on measurements of particle multiplicity at midrapidity [25].

In contrast, the centrality estimation using the energy measured at very large rapidity by the ZNA neutron calorimeter in the Pb-going direction introduces minimal bias. The ZNA detects slow neutrons emitted from nuclear deexcitation processes or knocked out by wounded nucleons [55,56]. The value of $N_{\rm part}$ is calculated using two procedures. The first one is that the energy spectrum obtained from the calorimeter is fitted by a Slow-Nucleon Emission model (which is developed based on the parametrization of results at lower energy p–A experiments [25,55]) coupled to the Glauber MC model. However, the estimation of $N_{\rm part}$ with this method is model-dependent. The second procedure is based on a hybrid method as discussed in detail in Ref. [25]. In this method, the values of $N_{\rm part}$ for each centrality class are obtained under the following assumptions:

$N_{\rm part}^{\text{high-}p_{\rm T}}$: The yield of high-$p_{\rm T}$ charged particles at midrapidity is proportional to the number of inelastic nucleon–nucleon collisions ($N_{\rm coll}$);
$N_{\rm part}^{\text{Pb-side}}$: The charged-particle multiplicity in the Pb-going direction is proportional to the number of wounded target nucleons.

The detailed calculations are discussed in Ref. [25]. The centrality classes used in this analysis are 0–5% (most central (higher multiplicity) collisions), 5–10%, 10–20%, 20–40%, 40–60%, 60–80% and 80–100% (most peripheral (lower multiplicity) collisions) for both CL1 and ZNA estimators.

5 Event generators and simulation framework

In the measurements of inclusive photon multiplicity, the corrections for instrumental effects and the evaluation of the systematic uncertainties are performed with the help of MC event generators. For p–Pb collisions, HIJING (v1.36) [57] and DPMJET (v3.0-5) [58] are used whereas PYTHIA 8 (v8.243) with the Monash 2013 tune [59] and EPOS LHC [60] are used for pp collisions. The generated particles from these event generators are transported through the experimental setup using the GEANT 3 software package [61], which includes a detailed description of the apparatus geometry and of the detector response via the AliRoot software framework [62]. The response of the PMD (in terms of the number of fired cells and energy deposition) to the incident particles in simulation is found to reproduce fairly well the results from the test beam data as discussed in Ref. [16].

For pp collisions 1 M (0.5 M) minimum bias INEL events were generated using the PYTHIA 8 (EPOS LHC) event generator whereas for p–Pb and Pb–p collisions 13.7 M (16 M)

and 3.4 M (1 M) NSD events were produced using HIJING (DPMJET).

The PYTHIA 8 [63] event generator is a standard tool for the generation of high energy physics collisions dominantly based on $2 \rightarrow 2$ hard scattering processes. In pp interactions, PYTHIA 8 introduces an impact-parameter dependent MultiParton Interaction (MPI) activity [64] to model the soft underlying event (UE). PYTHIA 8 uses the Lund string fragmentation model for the hadronization of partons. An MPI-based model is implemented in PYTHIA 8 to introduce beam remnants and color reconnection wherein all the gluons of lower-p_{T} interactions are merged with the color-flow dipoles of the highest-p_{T} one, in such a way that the total string length is minimized [65,66]. In the Monash tune of PYTHIA 8, the parameters relevant for initial-state radiation and MPI are tuned by using the MB, Drell-Yan, and UE data from the Tevatron, SPS and LHC. The EPOS event generator is a parton-based MC model with flux tube initial condition for hadron–hadron collisions. It uses Gribov–Regge theory for describing soft interactions. The EPOS LHC [60] generator is tuned to LHC data to describe the results from various collision systems at different center-of-mass energies, particularly the observed collective behavior in pp and p–Pb collisions at LHC energies.

The HIJING event generator is a pQCD inspired MC model aimed particularly at the study of jet and minijet production and jet-medium interactions in heavy-ion collisions. It also allows the study of particle production in high energy hadron–hadron and hadron–nucleus collisions. In p–A and heavy-ion collisions, multiple nucleon–nucleon interactions are simulated using binary approximation and the Glauber model. Nuclear shadowing effects are taken into account using parameterized parton distribution functions inside the nucleus. The soft interactions in HIJING are described by Lund FRITIOF [67] and the dual parton model (DPM) [68]. For jet fragmentation and hadronization, HIJING uses the prescription described in the Lund fragmentation model. The DPMJET event generator is a multi-purpose MC model based on the DPM capable of simulating hadron–hadron, hadron–nucleus, nucleus–nucleus, photon–hadron, photon–photon and photon–nucleus interactions from a few GeV up to the highest cosmic-ray energies. It uses the Glauber–Gribov multiple scattering formalisms to calculate nuclear cross sections and utilizes the Reggeon theory and pQCD to describe soft interactions and hard interactions respectively.

6 Photon reconstruction

A procedure similar to that described in Ref. [16] is adopted to reconstruct photons incident on the preshower plane of the PMD. An incident photon is expected to deposit a larger amount of energy (measured in ADC units) and produce a signal in a larger number of cells compared to an incident charged hadron on the PRE plane of the PMD. Using a nearest-neighbor clustering algorithm, contiguous cells having non-zero energy deposition are grouped together forming clusters. Each cluster carries information, such as the number of fired cells contained in the cluster, the position of the centroid of the cluster, and the total energy deposition in the cluster.

Suitable thresholds on the number of fired cells and the energy deposited in clusters are applied to discriminate between photon and hadron clusters. The number of clusters that satisfy the discrimination threshold conditions is termed as $N_{\gamma\text{-like}}$ clusters. A similar condition in discrimination threshold as used in Ref. [16], namely number of cells greater than 2 and energy deposition greater than 9 times the MPV (Most Probable Value of the charged pion ADC distribution from a Landau distribution function fitted to the data), is applied to obtain the distributions of $N_{\gamma\text{-like}}$ clusters. The $N_{\gamma\text{-like}}$ clusters provide a photon-rich sample, however, there are contaminations due to residual background from hadron clusters and from secondary particles (i.e. particles produced in interactions with the upstream material in front of the PMD) that reduce the purity of the sample. The application of the rejection criteria also removes some of the actual photons from the sample. The distributions of $N_{\gamma\text{-like}}$ clusters are therefore required to be corrected for these effects as discussed in the next section.

7 Correction procedure

The measured distributions of $N_{\gamma\text{-like}}$ clusters are distorted by several instrumental effects such as photon detection inefficiency, limited acceptance, contaminations from hadrons and secondary particles etc. A set of correction procedures is adopted to obtain the corrected N_{γ} distributions.

These instrumental effects are corrected for via a response matrix R_{mt} extracted from MC simulations using PYTHIA 8 with the Monash 2013 tune to generate pp collisions and the HIJING event generator for p–Pb collisions. These simulations include a detailed description of the experimental conditions and the detector settings and the simulated events are reconstructed and analyzed with the same algorithms used for the experimental data. Inelastic pp collisions can be classified into two processes: diffractive and non-diffractive (ND). The ND interactions are the dominant processes in pp collisions. According to Regge theory [69], diffractive scattering occurs via the exchange of Pomerons. In single diffractive (SD) processes, the exchanged Pomeron interacts and one of the protons breaks up, producing particles of the diffractive system of mass M_X. In double diffractive (DD) processes, both protons break up. It was found that the M_X distribution for the SD processes in experimental data [70,71] differs from the

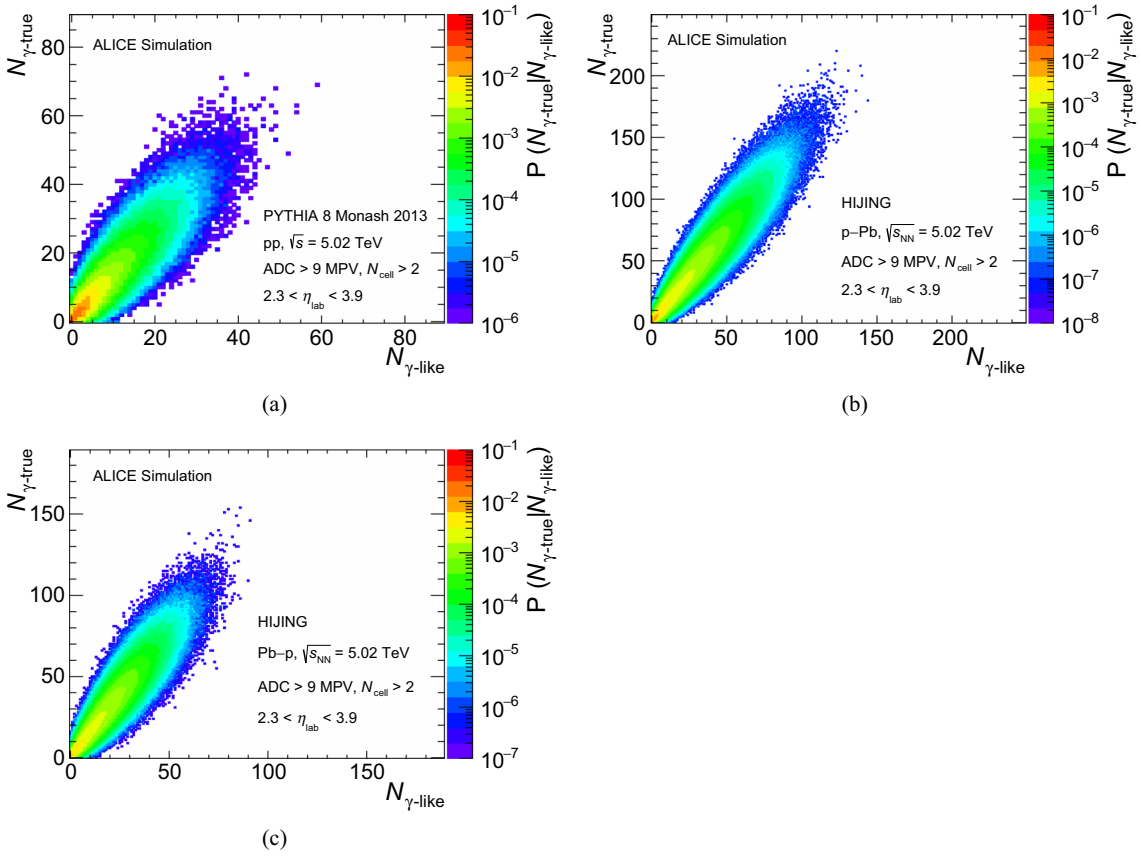

Fig. 1 Graphical representation of the detector response matrices for three different collision systems: pp (**a**), p–Pb (**b**) and Pb–p (**c**). The reconstructed and true photon multiplicities are denoted as $N_{\gamma\text{-like}}$ and $N_{\gamma\text{-true}}$, respectively, obtained from simulations using PYTHIA 8 with the Monash 2013 tune for pp collisions and HIJING for p–Pb and Pb–p collisions

one predicted by PYTHIA 8 simulations [72]. To account for this effect in simulation, diffraction-tuned event generators (which can reproduce diffraction cross sections and the shapes of the M_X distribution obtained from data) were used in previous charged-particle measurements by ALICE [22,23]. In this work, the M_X distribution of SD events in PYTHIA 8 with the Monash 2013 tune is reweighted to match the diffraction-tuned PYTHIA simulation used in previous 7 TeV analysis [22]. The response matrix in pp collisions is constructed using this reweighted PYTHIA 8 simulation.

Figure 1 shows the graphical representation of the detector response matrices for minimum bias pp, p–Pb, and Pb–p collisions in terms of the correlation between the true photon multiplicity ($N_{\gamma\text{-true}}$) from the event generator and the reconstructed photon multiplicity ($N_{\gamma\text{-like}}$) in the simulated events. The mean ($\langle N_{\gamma\text{-like}}\rangle$) and width ($\sigma_{N_{\gamma\text{-like}}}$) of the distribution of $N_{\gamma\text{-like}}$ are presented in Figs. 12 and 13 as a function of $N_{\gamma\text{-true}}$ for pp and p–Pb collisions at $\sqrt{s_{\rm NN}} = 5.02$ TeV. The resolution of photon multiplicity reconstruction in pp (p–Pb) collisions at $N_{\gamma\text{-true}} = 44(140)$ is found to be $\sim 12\%$ ($\sim 6\%$). Simulation studies have shown that the PMD is sensitive to transverse momenta ($p_{\rm T}$) as low as ~ 50 MeV/c [16]. In the correction procedure, true photons of all $p_{\rm T}$ are considered, which makes the present photon measurement inclusive. In simulation, the fraction of inclusive photons having $p_{\rm T}$ below 50 MeV/c is estimated to be about 16% for both pp and p–Pb collisions. The detection efficiency of inclusive photons as a function of η varies from 27% to 52%. The matrix element R_{mt} represents the conditional probability that an event with true multiplicity t is measured as an event with multiplicity m. The distorted measured distribution (M) can be expressed as

$$M = R_{mt}T. \tag{1}$$

One can therefore recover the true distribution (T) for given M as

$$T = R_{mt}^{-1}M. \tag{2}$$

However, the matrix R_{mt} may be singular and one can calculate inverse matrix R_{mt}^{-1} only if R_{mt} is not singular. Furthermore, even if R_{mt} can be inverted, the results obtained with Eq. 2 contain oscillations mainly because of finite statistics in the response matrix. To overcome this problem, a regularized unfolding method based on Bayes' theorem [73] using the

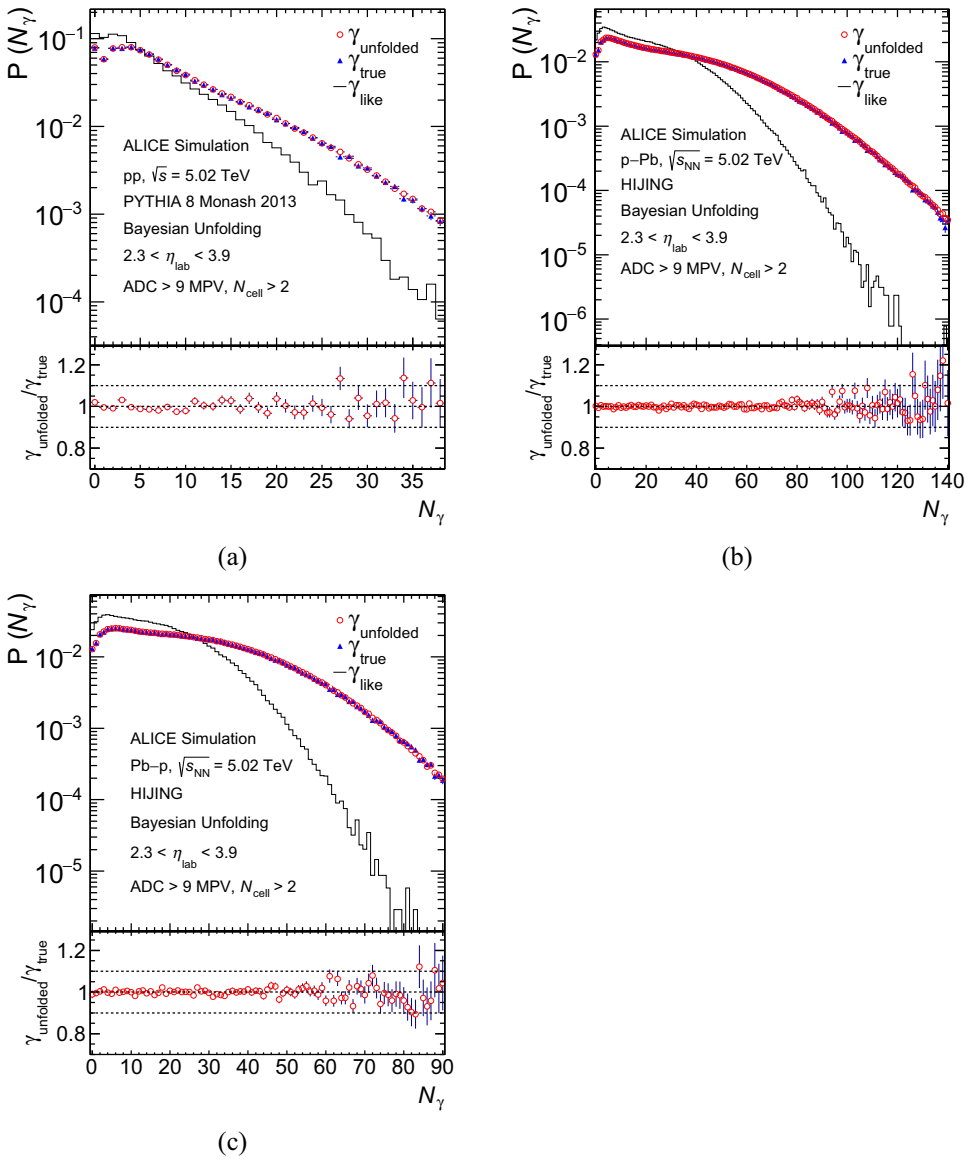

Fig. 2 MC closure test of the unfolding method for pp (**a**), p–Pb (**b**), and Pb–p (**c**) collisions at $\sqrt{s_{NN}} = 5.02$ TeV. The reconstructed, unfolded and true photon multiplicity distributions are presented in the top panels. The ratios of unfolded to true multiplicity distributions are shown in the bottom panels

RooUnfold software package [74] is used to correct the measured $N_{\gamma\text{-like}}$ distributions following the description outlined in Refs. [16,20–23].

In order to optimize the parameters (number of iterations) of the Bayesian unfolding method, a MC closure test was performed using simulations. The simulated data were divided into two statistically independent samples for the closure test. The response matrix was built using one set whereas the other set was used to obtain the reconstructed ($N_{\gamma\text{-like}}$) distributions, correct them using Eq. 2, and compare the result to the true distributions. The sensitivity of the results was checked by varying the number of iterations and a value corresponding to the best performance of the closure test was chosen as the optimized number of iterations. Figure 2 shows the performance of the closure tests for pp (Fig. 2(a)), p–Pb (Fig. 2(b)), and Pb–p (Fig. 2(c)) collisions. The upper panels show the true, reconstructed ($N_{\gamma\text{-like}}$), and unfolded photon multiplicity distributions. In the bottom panels, the ratios of the unfolded to the true photon multiplicity distributions are plotted for the optimized number of iterations (1 for pp, 4 for p–Pb, and 2 for Pb–p collisions). The ratio plots indicate that there is good agreement between the unfolded and true distributions except at high multiplicities where fluc-

Table 1 Trigger and vertex reconstruction efficiencies for INEL events in pp collisions and for NSD events in p–Pb and Pb–p collisions. Uncertainties listed are total uncertainties. Statistical uncertainties are negligible

System	Trigger efficiency (%)	Vertex reconstruction efficiency (%)
pp	94.5 ± 1.2	95.0 ± 0.6
p–Pb	98.5 ± 0.9	99.8 ± 0.1
Pb–p	98.5 ± 0.9	99.8 ± 0.1

tuations arise due to the limited size of the simulated sample. The measured photon distributions in experimental data were unfolded using the optimized number of iterations. An alternate method of unfolding, singular value decomposition (SVD) [75], was also used and consistent results were obtained. In this method, the response matrix can be factorized in the form $R_{mt} = USV^T$, where U and V are orthogonal matrices and S is a diagonal matrix with non-negative diagonal elements. These diagonal elements are called singular values of the matrix R_{mt}. Regularization is applied by using a smooth cut-off on small singular-value contributions suppressing large fluctuations in the unfolded distribution. The same procedure was applied to extract the pseudorapidity distributions, but the unfolding of photon multiplicity distributions was performed separately in eight pseudorapidity intervals of a width of 0.2 units.

The unfolded results in MB collisions are then corrected for the trigger ($\epsilon_{\rm Trig}$) and vertex reconstruction ($\epsilon_{\rm Vtx}$) efficiencies. A similar procedure as discussed in [16] is adopted to estimate $\epsilon_{\rm Trig}$ and $\epsilon_{\rm Vtx}$ using MC simulations. These efficiencies can be defined as

$$\epsilon_{\rm Trig} = \frac{N_{\rm Trig}}{N_{\rm All}}, \quad \epsilon_{\rm Vtx} = \frac{N_{\rm TrigVtx}}{N_{\rm Trig}} \tag{3}$$

where $N_{\rm All}$ and $N_{\rm Trig}$ correspond to the number of all simulated events and of triggered events, respectively, and $N_{\rm TrigVtx}$ corresponds to triggered events with reconstructed vertex. The values of $\epsilon_{\rm Trig}$ and $\epsilon_{\rm Vtx}$ for pp, p–Pb, and Pb–p collisions are reported in Table 1. The unfolded pseudorapidity distributions are corrected for these efficiencies using an overall correction factor whereas multiplicity dependent correction factors are used to correct the multiplicity distributions.

The V0-AND trigger used to select p–Pb events is not fully efficient for NSD events. The correction for the V0-AND trigger inefficiency and the imperfect description in the MC of the vertex reconstruction efficiency would mainly concern the most peripheral event class (80–100%). In this work, centrality classes have been defined as percentiles of the visible cross section and the centrality dependent pseudorapidity distributions are not corrected for trigger inefficiencies as was also reported in Ref. [25].

8 Estimation of systematic uncertainties

The contributions of the different sources of systematic uncertainties associated with the measurements of multiplicity and pseudorapidity distributions of inclusive photons are summarized in Table 2 for the measurements in MB events of pp, p–Pb, and Pb–p collisions and in Tables 3 and 4 for the measurements in centrality classes of p–Pb collisions. The results of p–Pb collisions in centrality classes are not affected by the uncertainties on the event selection and diffraction mass. The total systematic uncertainties are calculated by adding the contributions from the individual sources in quadrature. The methods used for the estimation of the systematic uncertainties are discussed in the following subsections.

8.1 Effect of upstream material

One of the major contributions to the systematic uncertainties comes from the uncertainty in the implementation of upstream material in front of the PMD (i.e., the material between the nominal IP and the PMD) in the GEANT 3

Table 2 Contributions to systematic uncertainties (in percent) in the measurements of pseudorapidity and multiplicity distributions of inclusive photons in pp, p–Pb, and Pb–p collisions. For multiplicity distributions, numbers are given at multiplicity values of 0, the mean $\langle m \rangle$ and when $P(N_\gamma) = 10^{-3}$

Sources	$dN_\gamma/d\eta_{\rm lab}$ analysis			$P(N_\gamma)$ analysis								
	pp	p–Pb	Pb–p	pp			p–Pb			Pb–p		
				N_γ 0	N_γ $\langle m \rangle$	$P(N_\gamma)$ 10^{-3}	N_γ 0	N_γ $\langle m \rangle$	$P(N_\gamma)$ 10^{-3}	N_γ 0	N_γ $\langle m \rangle$	$P(N_\gamma)$ 10^{-3}
Upstream material	7.0	8.2–10.1	8.7–9.9	3.0	2.5	20.0	15.2	3.4	34.0	18.5	3.7	37.2
Hadron and secondary contamination	1.9	1.9	2.0	1.4	1.4	7.5	6.7	1.2	1.2	0.7	1.1	7.2
Event generator for response matrix	2.5	3.2	1.0	2.6	3.0	5.0	3.2	3.6	16.0	3.0	3.5	14.4
Unfolding method	3.1	0.6	1.1	25.0	3.7	23.0	11.0	1.2	1.2	11.0	3.0	3.0
Event selection efficiency	1.2	0.9	0.9	19.0	1.6	1.6	33.5	1.2	0.7	34.0	1.0	0.8
Diffraction shape	2.1	n/a	n/a	1.3	4.0	5.3	n/a	n/a	n/a	n/a	n/a	n/a
Diffraction ratio	2.3	n/a	n/a	7.4	4.6	0.2	n/a	n/a	n/a	n/a	n/a	n/a
Total	8.9	9.1–10.8	9.1–10.2	32.8	8.4	32.0	39.3	5.4	37.6	40.3	6.0	40.7

Table 3 Contributions to systematic uncertainties (in percent) in the measurements of centrality dependent pseudorapidity distributions of inclusive photons using the CL1 estimator in p–Pb collisions

Sources	0–5%	5–10%	10–20%	20–40%	40–60%	60–80%	80–100%
Upstream material	8.2–10.1	8.2–10.1	8.2–10.1	8.2–10.1	8.2–10.1	8.2–10.1	8.2–10.1
Hadron and secondary contamination	2.1	2.3	2.1	2.3	2.4	2.1	3.1
Event generator for response matrix	3.0	3.0	3.1	3.0	2.9	3.1	3.0
Unfolding method	1.7	2.9	2.6	2.9	3.1	2.8	2.8
Total	9.2–10.9	9.5–11.2	9.4–11.0	9.5–11.1	9.6–11.2	9.5–11.1	9.7–11.3

Table 4 Contributions to systematic uncertainties (in percent) in the measurements of centrality dependent pseudorapidity distributions of inclusive photons using the ZNA estimator in p–Pb collisions

Sources	0–5%	5–10%	10–20%	20–40%	40–60%	60–80%	80–100%
Upstream material	8.2–10.1	8.2–10.1	8.2–10.1	8.2–10.1	8.2–10.1	8.2–10.1	8.2–10.1
Hadron and secondary contamination	2.1	1.3	1.6	1.6	2.1	1.7	2.6
Event generator for response matrix	1.4	1.8	2.2	3.2	3.8	3.3	2.7
Unfolding method	2.8	1.9	2.0	1.7	2.7	2.8	3.0
Total	9.1–10.8	8.7–10.5	9.0–10.7	9.2–10.9	9.7–11.3	9.5–11.1	9.6–11.2

description of the ALICE apparatus. At forward rapidity, the material budget was studied in detail for the charged-particle multiplicity measurements [23,30,31]. Based on this study, an upper limit of the material budget uncertainty of 10% was considered in this analysis. To study the effect of this on photon counting in p–Pb and Pb–p collisions, two response matrices using the HIJING event generator were considered, one with the default material description and the other with a 10% increase in the overall material of the ALICE apparatus. The measured distribution in data is then unfolded using these two different matrices. The difference between the two unfolded multiplicities determines the systematic uncertainty due to the material in front of the PMD. A similar procedure is applied for each $\eta_{\rm lab}$ interval to obtain the systematic uncertainties for the pseudorapidity distributions of inclusive photons in MB events and in all centrality classes. The systematic uncertainty due to material effects for pp collisions is taken from the previously published paper on inclusive photon measurement in pp collisions at $\sqrt{s}$ = 0.9, 2.76, and 7 TeV [16].

8.2 Contamination in the photon sample

The photon–hadron discrimination conditions in terms of energy deposition and number of cells in clusters were optimized to minimize contaminations from hadronic clusters and secondary particles. The purity of the photon sample with the default threshold condition (energy deposition greater than 9 times the MPV and number of cells greater than 2) is found to be 65%. To estimate the systematic uncertainty due to the correction for the contamination, the analysis was repeated with a different threshold condition on energy deposition (greater than 6 times the MPV). The unfolded distributions are obtained for both cases and the difference between these two distributions is quoted as the systematic uncertainty. By applying a higher threshold condition on energy deposition (greater than 12 times the MPV), the estimated systematic uncertainty with respect to the default threshold condition is found to be of the same order as the quoted one.

8.3 Unfolding procedure

As discussed in Sect. 7, we rely on MC models to unfold the measured photon multiplicity and pseudorapidity distributions. The sensitivity of the unfolded results to the choice of the MC models used in the unfolding procedure is estimated by comparing the results obtained using the response matrices from two different event generators. For pp collisions, two separate response matrices are built using PYTHIA 8 with the Monash 2013 tune and EPOS LHC, whereas for p–Pb and Pb–p collisions those are constructed using HIJING and DPMJET. These matrices are used to unfold the measured distributions in data. The difference in the unfolded distributions is considered as the systematic uncertainty. The effect of the choice of the unfolding method was determined by using an alternative unfolding method, SVD, in addition to the default Bayesian method. The difference in the unfolded results is considered as the systematic uncertainty.

8.4 Event selection efficiency

The systematic uncertainty due to possible imperfections in the correction for the event selection efficiency is determined by estimating the trigger and vertex reconstruction efficiencies using two different event generators. For pp collisions, the efficiency values are computed from events simulated with the PYTHIA 8 with Monash 2013 tune and EPOS LHC generators, while HIJING and DPMJET are used to obtain these efficiencies in p–Pb and Pb–p collisions. This uncertainty mostly influences the zero multiplicity bin in the multiplicity distributions and it reduces significantly at large multiplicity because single and double diffraction contributions become smaller when going to higher multiplicity.

8.5 Diffraction mass distributions

As described in Sect. 7, the central values of the final results in pp collisions are determined using simulations with the PYTHIA 8 event generator with the Monash 2013 tune reweighted to match the measured M_X distribution in SD events. The uncertainty associated with this procedure is estimated by taking the difference between the results obtained with the reweighted mass distribution and the default one from PYTHIA 8 with Monash 2013 tune. The uncertainty related to the fractions of SD and DD events produced by PYTHIA 8 is also evaluated by varying those fractions by ± 30% of their nominal values.

9 Results and discussions

The multiplicity and pseudorapidity distributions of inclusive photons in the forward pseudorapidity interval $2.3 < \eta_{\rm lab} < 3.9$ measured using the PMD for pp collisions at $\sqrt{s} = 5.02$ TeV and p–Pb and Pb–p collisions at $\sqrt{s_{\rm NN}} = 5.02$ TeV are presented and discussed in this section. The distributions are obtained without any selection on the transverse momentum of the photons. The obtained results are compared with predictions from MC models and available experimental measurements of charged particles.

9.1 Multiplicity distributions

The measured multiplicity distributions of inclusive photons are presented as probability distributions ($\mathrm{P}(N_\gamma)$) as a function of N_γ in Fig. 3. The systematic uncertainty is represented by the gray bands and the statistical uncertainty is smaller than the marker size. The measurements are obtained for pp and for both configurations of p–Pb collisions in the pseudorapidity interval $2.3 < \eta_{\rm lab} < 3.9$. The average photon multiplicity for pp collisions is 6.44 ± 0.36 (sys), for p–Pb collisions is 29.38 ± 1.88 (sys), and for Pb–p collisions is 24.59 ± 1.52 (sys). The multiplicity range in p–Pb collisions reaches up to 140 which is about 5 times larger than its mean multiplicity. The average multiplicity in pp collisions is about 4.5 times smaller than that in p–Pb collisions. The different multiplicity distributions and average values in p–Pb and Pb–p collisions arise from the different particle production in the p-going and Pb-going hemispheres as well as from the difference in the rapidity coverage of the PMD in the center-of-mass frame because of the Δy shift of ± 0.465 units between p–Pb and Pb–p collisions.

The results in pp collisions (Fig. 3(a)) are compared to the predictions from PYTHIA 8 with the Monash 2013 tune [59], PYTHIA 6 (v6.425) with the Perugia 2011 tune [76], PHOJET (v1.12) [77], and EPOS LHC [60] event generators. The ratios between MC predictions and data are shown in the bottom panels. It is observed that PYTHIA 8 with the Monash 2013 tune and EPOS LHC are unable to reproduce the inclusive photon production in pp collisions at $\sqrt{s} = 5.02$ TeV at high multiplicities. On the other hand, the Perugia 2011 tune of PYTHIA 6 and PHOJET are found to fairly describe the data within uncertainties.

The multiplicity distributions in p–Pb collisions (Fig. 3(b)) are compared to predictions obtained from HIJING, DPMJET, and AMPT (v2.25) [78]. None of the models could reproduce the shape of the distributions in the full multiplicity range. HIJING is closer to the data points at intermediate multiplicities. The tail of the distribution at high multiplicity can be described by both HIJING and AMPT models within uncertainties. For Pb–p collisions (Fig. 3(c)), DPMJET strongly underestimates the data at high multiplicity. HIJING describes the data slightly better in the full range of multiplicity compared to AMPT.

These experimental results are expected to provide new constraints on inclusive photon production mechanisms implemented in theoretical models.

In Fig. 4, the measured multiplicity distributions are fitted by a weighted sum of two negative binomial distributions (NBDs) (Eq. 4) to extract the relative contributions from soft and semihard processes in the particle production mechanisms. In Eq. 4, the subscripts and superscripts in the parameters indicate the respective components. The $\alpha_{\rm soft}$ parameter gives the fraction of soft events. The NBD distribution, $\mathrm{P_{NBD}}$, has the following parameters: the average multiplicity $\langle n \rangle$, which is found to increase with increasing $\sqrt{s}$, and the shape parameter, k, which decreases with increasing $\sqrt{s}$ in hadronic collisions [16,22,23].

$$\mathrm{P}(n) = \lambda[\alpha_{\rm soft}\mathrm{P_{NBD}}(n, \langle n^{\rm soft}\rangle, k^{\rm soft}) + (1-\alpha_{\rm soft})\mathrm{P_{NBD}}(n, \langle n^{\rm semihard}\rangle, k^{\rm semihard})] \quad (4)$$

where

$$\mathrm{P_{NBD}}(n, \langle n\rangle, k) = \frac{\Gamma(n+k)}{\Gamma(k)\Gamma(n+1)} \frac{(\langle n\rangle/k)^n}{(1+\langle n\rangle/k)^{n+k}}. \quad (5)$$

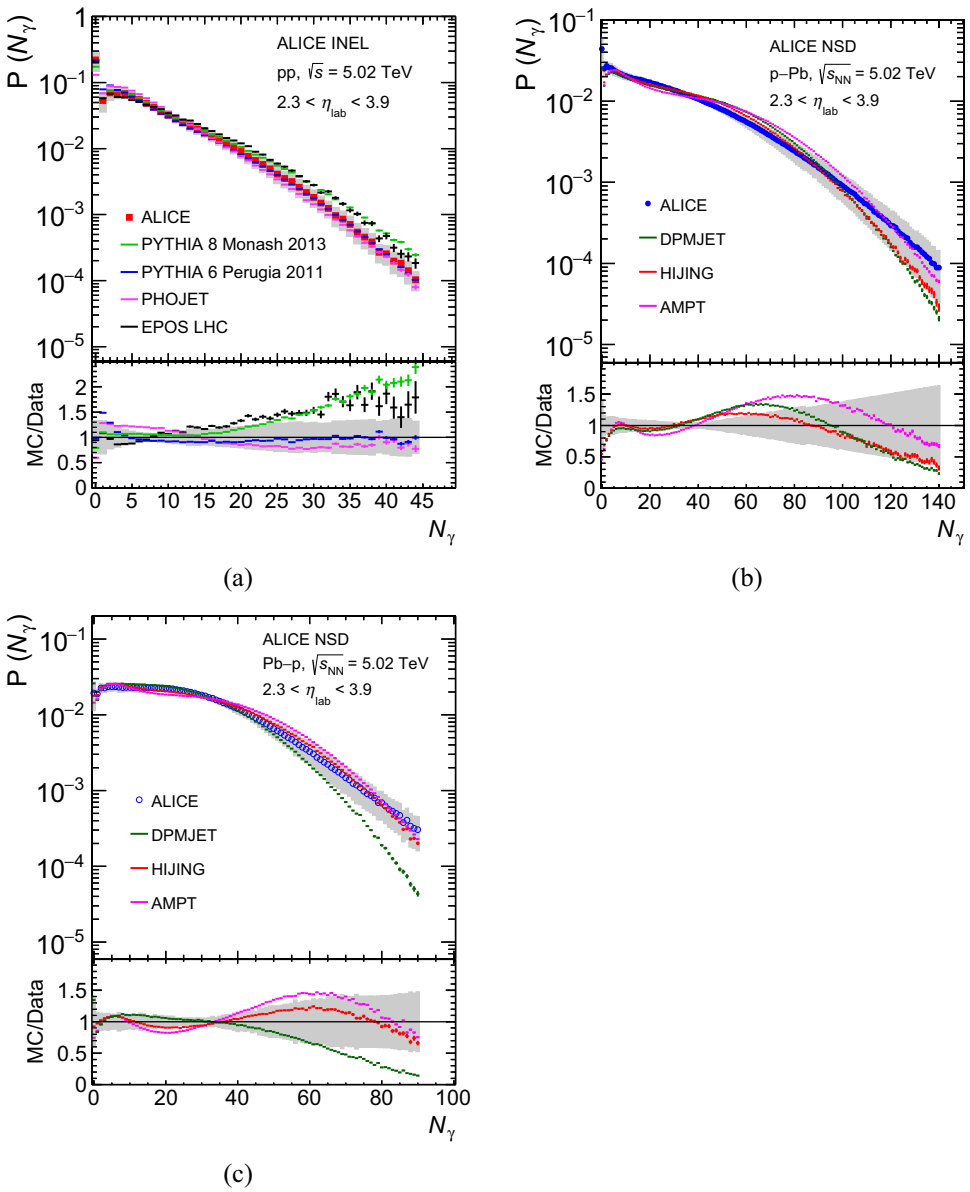

Fig. 3 Top panels: Inclusive photon multiplicity distributions measured within $2.3 < \eta_{\rm lab} < 3.9$ in pp (**a**), p–Pb (**b**), and Pb–p (**c**) collisions at $\sqrt{s_{\rm NN}} = 5.02$ TeV. Results from various MC predictions are superimposed. Bottom panels: The ratios between MC results and data are shown. Shaded boxes represent the systematic uncertainties

Double NBDs do not describe the value P(0), therefore, the bin $N_\gamma = 0$ was excluded from the fit and a normalization factor λ was introduced to account for this. The systematic uncertainties associated with (a) the change of photon–hadron discrimination thresholds, (b) the tuning of event generator for diffraction, (c) the effect of upstream material, and (d) the correction of event selection efficiency produce a correlated shift of the multiplicity distributions. These correlated uncertainties are therefore not considered in the fitting procedure. The other sources of systematic uncertainties (uncorrelated) are taken into account in the fit. The obtained parameters from these fits are printed in bold in Table 5. The other set of parameters reported in Table 5 is obtained from the fitting of the data by considering both correlated and uncorrelated uncertainties to provide an estimate of how much the fit parameters change due to the presence of correlations in the systematic uncertainties.

The double NBD fit describes the data within uncertainties. The results show an increase in the mean multiplicity of inclusive photons with system size whereas the shape parameter decreases with system size. Moreover, it is observed that $\langle n^{\rm semihard}\rangle \approx 3\langle n^{\rm soft}\rangle$ which is consistent with the results of charged-particle production at central and forward rapidities in pp collisions [22,23].

9.2 Pseudorapidity distributions in NSD and INEL events

The pseudorapidity distributions of inclusive photons measured within $2.3 < \eta_{\rm lab} < 3.9$ in pp, p–Pb, and Pb–p collisions are presented in Fig. 5. The gray bands represent

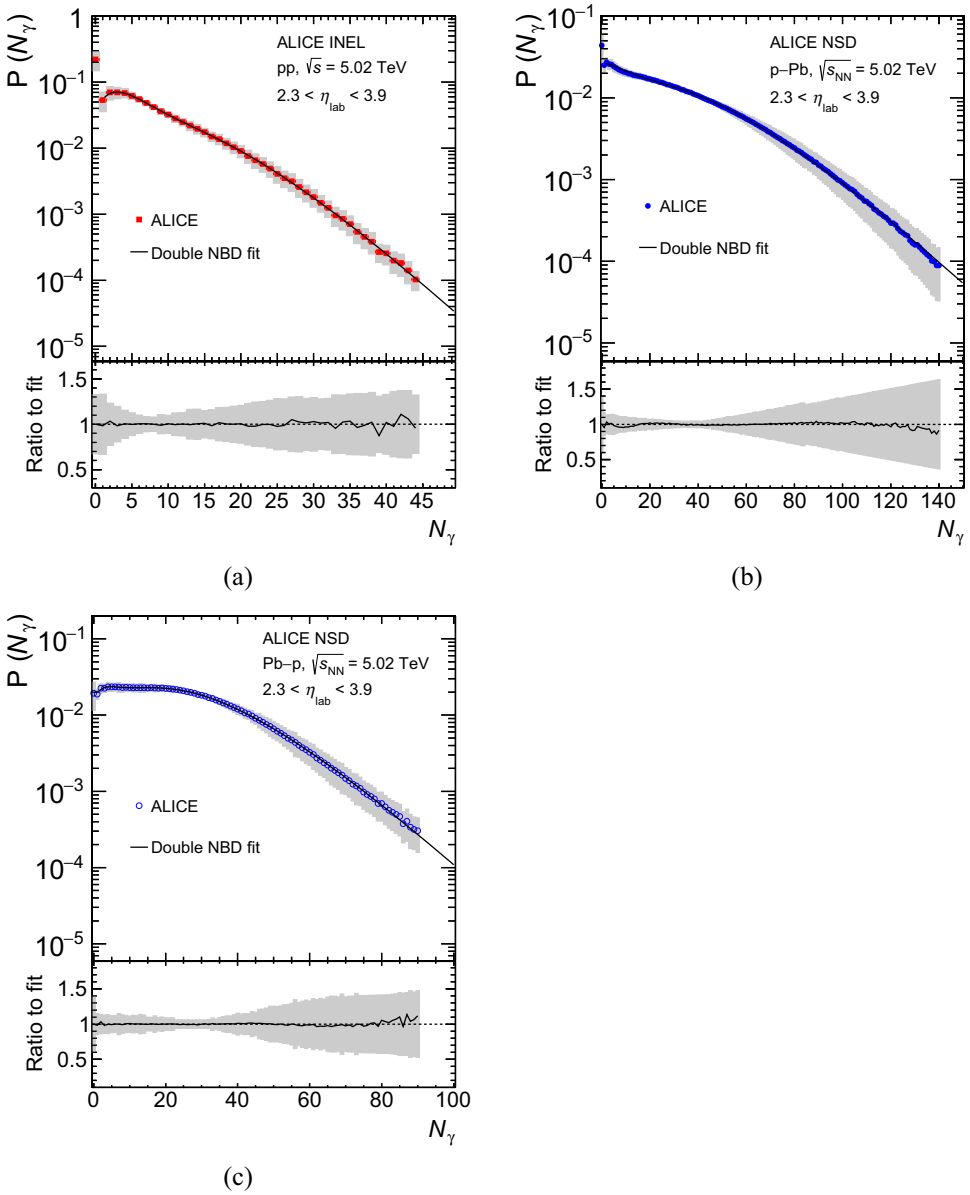

Fig. 4 Top panels: multiplicity distribution of inclusive photons fitted to double NBDs for pp (**a**), p–Pb (**b**), and Pb–p (**c**) collisions at $\sqrt{s_{NN}} = 5.02$ TeV. Bottom panels: the ratio of the data to the fit is presented. Shaded boxes represent the systematic uncertainties

Table 5 Double NBD fit parameters for the inclusive photon multiplicity distributions. The obtained parameters from fits to the data by considering only uncorrelated uncertainties are printed in bold. The other set of parameters is obtained when both correlated and uncorrelated uncertainties are considered in the fitting procedure

Collision system	λ	α_{soft}	k^{soft}	$\langle n^{soft} \rangle$	$k^{semihard}$	$\langle n^{semihard} \rangle$
pp	**0.79 ± 0.03**	**0.60 ± 0.19**	**2.97 ± 1.16**	**4.65 ± 1.01**	**4.56 ± 1.79**	**13.47 ± 2.60**
	0.79 ± 0.04	0.61 ± 0.28	2.97 ± 1.74	4.67 ± 1.60	4.64 ± 2.76	13.55 ± 4.07
Pb–p	**0.99 ± 0.01**	**0.29 ± 0.10**	**1.65 ± 0.30**	**8.92 ± 2.10**	**4.09 ± 0.39**	**31.08 ± 1.31**
	0.99 ± 0.01	0.31 ± 0.13	1.60 ± 0.33	9.70 ± 4.00	4.22 ± 0.65	31.56 ± 2.14
p–Pb	**0.99 ± 0.01**	**0.62 ± 0.10**	**1.10 ± 0.05**	**18.76 ± 2.50**	**3.89 ± 0.30**	**47.21 ± 1.28**
	0.98 ± 0.01	0.60 ± 0.11	1.10 ± 0.10	18.80 ± 3.60	3.64 ± 0.40	46.18 ± 1.72

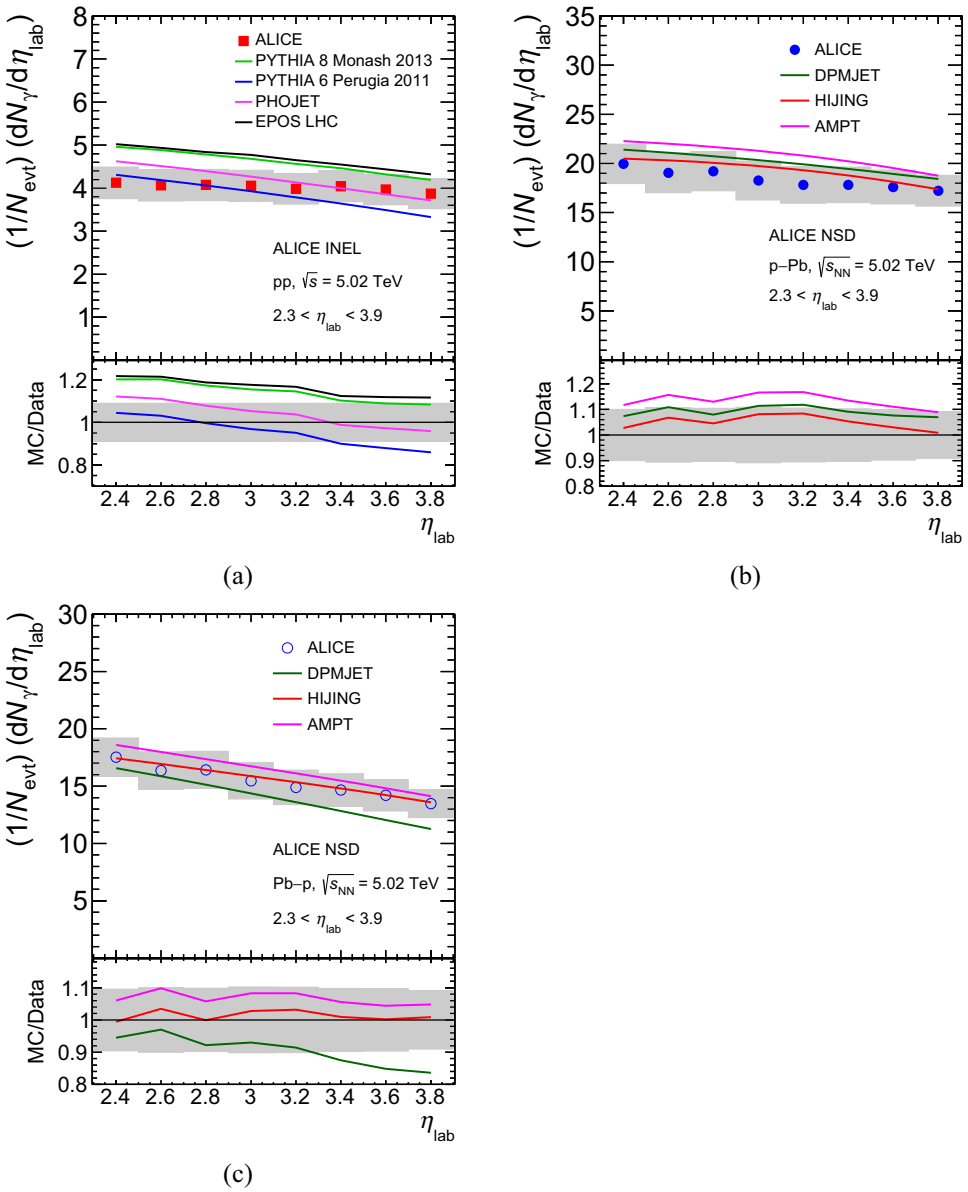

Fig. 5 Top panels: pseudorapidity distribution of inclusive photons measured within $2.3 < \eta_{\rm lab} < 3.9$ in pp (**a**), p–Pb (**b**), and Pb–p (**c**) collisions at $\sqrt{s_{\rm NN}} = 5.02$ TeV. Results from various MC predictions are superimposed. Bottom panels: the ratios between MC results and data are shown. Shaded boxes represent the systematic uncertainties

the systematic uncertainty and the statistical uncertainty is smaller than the marker size. The measurements are compared to the predictions from MC event generators and the ratios between MC results and data are shown in the bottom panels.

In pp collisions (Fig. 5(a)), PHOJET and PYTHIA 6 with the Perugia 2011 tune models show better agreement with the data compared to EPOS LHC and PYTHIA 8 with the Monash 2013 tune. All model predictions are however found to be compatible within about 20% from the measured values, but the $\eta_{\rm lab}$ dependence is flatter in the data than in the models.

In p–Pb collisions the value of pseudorapidity density of inclusive photons is found to be slightly larger than that for Pb–p collisions as expected due to the fact that the PMD measures particles produced in the Pb-going direction in the former configuration and in the p-going direction in the latter, and also due to the different rapidity ranges covered by the PMD in the center-of-mass frame for p–Pb and Pb–p collisions as discussed in Sect. 9.1. The data are compared to several models with different descriptions of particle production, all shifted by $\Delta y = 0.465$ to take into account the shift to the laboratory system. It is observed that HIJING describes both p–Pb and Pb–p results within systematic uncertainties. AMPT overpredicts the data in the Pb-going side and reproduces the measurements within uncertainties in the p-going side. DPMJET underestimates the multiplicity in the p-going side. One can observe that the DPMJET curve lies in between AMPT and HIJING in the Pb-going side and goes below in the p-going side. This suggests that DPMJET predicts a slightly narrower distribution. It is also noted that all models lie within about 15% from the data points.

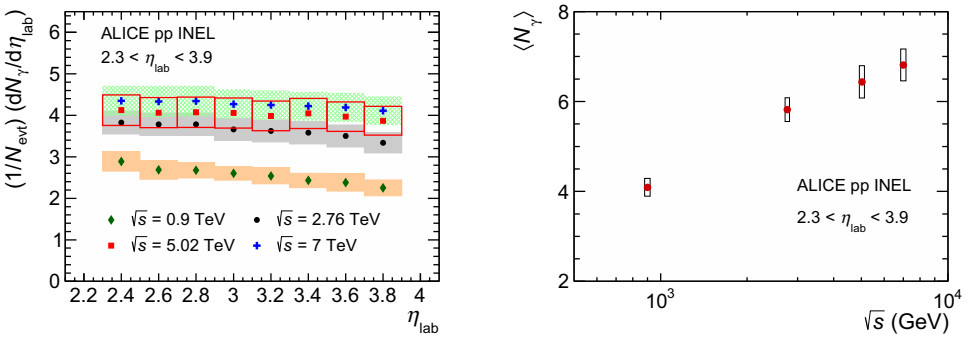

Fig. 6 (**a**) Comparison of $\mathrm{d}N_\gamma/\mathrm{d}\eta_{\mathrm{lab}}$ measured at forward rapidity in INEL pp collisions for various center-of-mass energies, (**b**) average photon multiplicity within $2.3 < \eta_{\mathrm{lab}} < 3.9$ as a function of collision energy in INEL pp collisions. The results at 0.9, 2.76, and 7 TeV are taken from Ref. [16]

Table 6 The average photon multiplicity $\langle N_\gamma \rangle$ within $2.3 < \eta_{\mathrm{lab}} < 3.9$ for various center-of-mass energies in INEL pp collisions. The quoted errors are systematic uncertainties. Statistical uncertainties are negligible. Data points at 0.9, 2.76, and 7 TeV are taken from Ref. [16]

$\sqrt{s}$ (TeV)	$\langle N_\gamma \rangle$
0.9	4.09 ± 0.20
2.76	5.82 ± 0.26
5.02	6.44 ± 0.36
7	6.81 ± 0.35

The same models that do not reproduce the high-multiplicity part of the $\mathrm{P}(N_\gamma)$ distribution in MB collisions, provide a fair description of the multiplicity of inclusive photons, $\mathrm{d}N_\gamma/\mathrm{d}\eta_{\mathrm{lab}}$, at forward rapidities in pp, p–Pb, and Pb–p collisions.

The simultaneous comparison of the measured $\mathrm{P}(N_\gamma)$ and $\mathrm{d}N_\gamma/\mathrm{d}\eta_{\mathrm{lab}}$ distributions to the predictions of different event generators has therefore the potential of further constraining the models of inclusive photon production in high energy hadronic collisions.

The $\mathrm{d}N_\gamma/\mathrm{d}\eta_{\mathrm{lab}}$ distributions measured in the rapidity interval $2.3 < \eta_{\mathrm{lab}} < 3.9$ in INEL pp collisions at various center-of-mass energies are compared in Fig. 6(a). Two additional systematic uncertainties (diffraction shape and diffraction ratio) are considered in this analysis and they lead to a total systematic uncertainty that is slightly larger at $\sqrt{s} = 5.02$ TeV with respect to the other energies. However, the total systematic uncertainty at all energies mostly comes from the 10% uncertainty on the upstream material in front of the PMD. The material uncertainty shows essentially no $\sqrt{s}$ variation and is therefore fully correlated over all energies. A smooth increase of the inclusive photon multiplicity with increasing collision energy is observed. The average photon multiplicity $\langle N_\gamma \rangle$ within $2.3 < \eta_{\mathrm{lab}} < 3.9$ as a function of $\sqrt{s}$ is shown in Fig. 6(b). The results of the measurements of $\langle N_\gamma \rangle$ are given in Table 6.

Since the dominant contribution to inclusive photon production comes from π^0 decays, the number of produced photons should be similar to the charged-particle multiplicity. The comparison between the pseudorapidity distribution of inclusive photons in INEL pp and NSD p–Pb (combined with results of Pb–p mirrored with respect to $\eta_{\mathrm{lab}} = 0$) events measured at forward rapidity and that of charged particles at midrapidity by ALICE [24,79] and CMS [41] are presented in Fig. 7. It is observed that the inclusive photon production at forward rapidity follows the trend of charged-particle production at midrapidity. The predictions from the different event generators are also displayed in Fig. 7 and they show similar values for charged-particle (dashed lines) and photon (solid lines) multiplicity at forward and backward pseudorapidities, while at midrapidity the photon and charged-particle pseudorapidity density differ. The origin of this difference is due to a mass effect in the transformation between $\mathrm{d}N/\mathrm{d}y$ and $\mathrm{d}N/\mathrm{d}\eta$ at $\eta \approx 0$. The measured $\mathrm{d}N_{\mathrm{ch}}/\mathrm{d}\eta_{\mathrm{lab}}$ in p–Pb collisions is well described by both HIJING and DPMJET event generators. HIJING reproduces better the $\mathrm{d}N_\gamma/\mathrm{d}\eta_{\mathrm{lab}}$ compared to DPMJET. For pp collisions, both PYTHIA 8 with the Monash 2013 tune and EPOS LHC overpredict the photon and charged-particle multiplicity.

9.3 Pseudorapidity distributions in centrality classes of p–Pb collisions

The pseudorapidity distributions of inclusive photons as a function of pseudorapidity measured in p–Pb collisions are presented in Fig. 8 for several centrality classes estimated using two centrality estimators, CL1 (top) and ZNA (bottom). The analysis was not performed for the Pb–p configuration, hence only one rapidity interval is covered for the photon measurements, namely the one in the Pb-going direction, and the ZNA measures the energy of the neutrons emitted in the direction of the Pb beam. The multiplicity in the most central (0–5%) collisions when considering the CL1 (ZNA) estimator reaches ~ 3 (~ 2) times larger value compared to that measured in MB events. The lower values of $\mathrm{d}N_\gamma/\mathrm{d}\eta_{\mathrm{lab}}$ in case of central events selected with the ZNA estimator is, most probably, due to the saturation of forward neutron emission [25]. The systematic uncertainty represented by open boxes mostly comes from the uncertainty on the upstream material in front of the PMD. To understand further the evo-

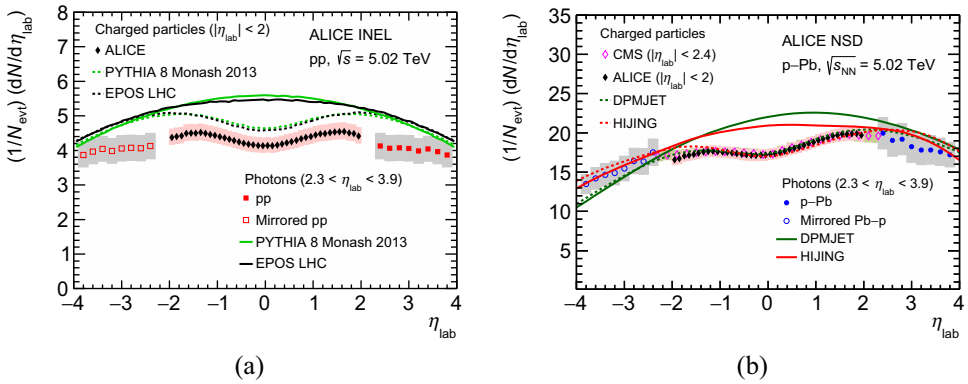

Fig. 7 The pseudorapidity distributions of inclusive photons are compared with charged-particle measurements at midrapidity by ALICE [79] in pp collisions (**a**) and both ALICE [24] and CMS [41] in p–Pb collisions at $\sqrt{s_{NN}} = 5.02$ TeV (**b**). Mirrored data points of pp and Pb–p results and predictions from various MC models are superimposed

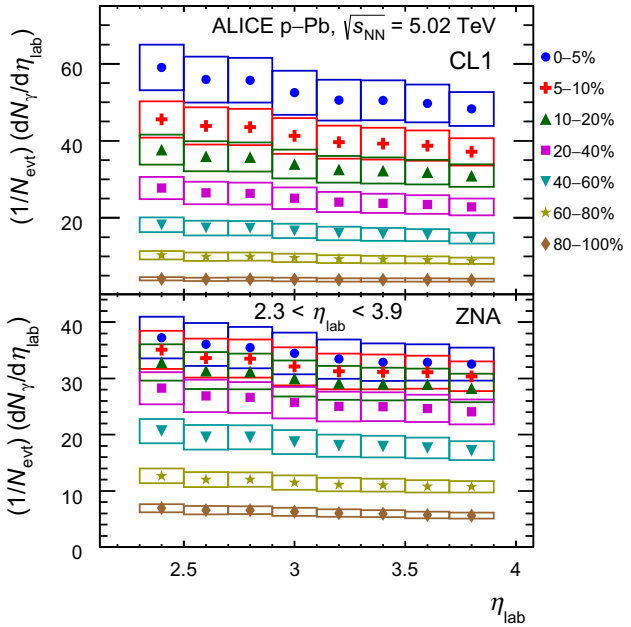

Fig. 8 Pseudorapidity distributions of inclusive photons measured within $2.3 < \eta_{lab} < 3.9$ in p–Pb collisions at $\sqrt{s_{NN}} = 5.02$ TeV for several centrality classes and for two centrality estimators: CL1 (top) and ZNA (bottom)

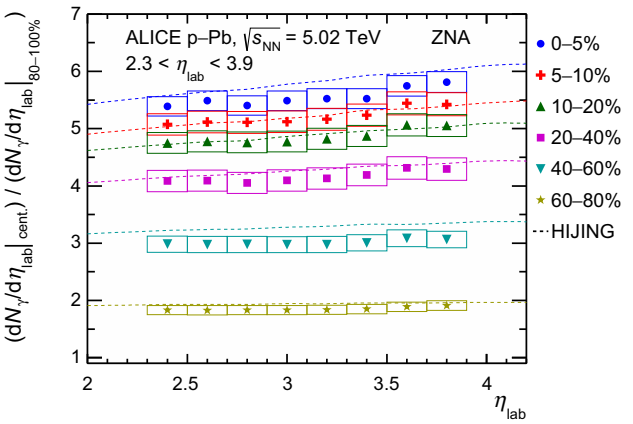

Fig. 9 Ratios of $dN_\gamma/d\eta_{lab}$ distributions measured in different centrality classes to that in the most peripheral (80–100 %) centrality class. The corresponding HIJING predictions are shown by dotted lines

lution of $dN_\gamma/d\eta_{lab}$ with centrality the distributions in each centrality interval are divided by the distribution in the most peripheral (80–100%) event class and presented in Fig. 9. With increasing pseudorapidity the ratios are observed to increase linearly with a slope whose magnitude increases for central events being highest for the most central (0–5%) collisions. HIJING shows a similar trend and explains the data within measured uncertainties except for the 0–5% and 40–60% event classes.

The results are compared in Fig. 10 to similar measurements of charged particles at midrapidity by ALICE [25] for selected centrality intervals (0–5%, 20–40% and 80–100%) determined with the CL1 (top panel) and ZNA (bottom panel) estimators. A clear asymmetric shape of $dN_{ch}/d\eta_{lab}$ is observed for most central collisions and the shape becomes symmetric (like in pp) in the most peripheral event class. Figure 10 also reports the comparison of the measured $dN_\gamma/d\eta_{lab}$ with HIJING predictions for the three considered centrality classes. The $dN_{ch}/d\eta_{lab}$ distributions at midrapidity are better described by the model in the case of the ZNA estimator. In the most peripheral (80–100%) collisions, HIJING overpredicts (underpredicts) the $dN_{ch}/d\eta_{lab}$ for the CL1 (ZNA) estimator. The model describes the values of $dN_\gamma/d\eta_{lab}$ at forward rapidity to within 15% except for the 0–5% CL1 class and the 80–100% ZNA class where the model prediction is compatible with the data points within 5%.

The obtained values of average photon multiplicity $\langle N_\gamma \rangle$ at forward rapidity ($2.3 < \eta_{lab} < 3.9$) as a function of $\langle N_{part} \rangle$ for the two centrality estimators in p–Pb collisions at $\sqrt{s_{NN}} = 5.02$ TeV are presented in Fig. 11(a) and listed in Table 7. The systematic uncertainties are represented by the color bands. The values of $\langle N_{part} \rangle$ for the different centrality classes for both the estimators are taken from [25]. The data point for pp collisions at $\sqrt{s} = 5.02$ TeV is also included for reference. The average photon multiplicity $\langle N_\gamma \rangle$ divided by the average number of participants is presented as a function of $\langle N_{part} \rangle$ in Fig. 11(b). The $\langle N_\gamma \rangle / \langle N_{part} \rangle$ ratio has a steeper increase with $\langle N_{part} \rangle$ for the CL1 centrality estimator than for

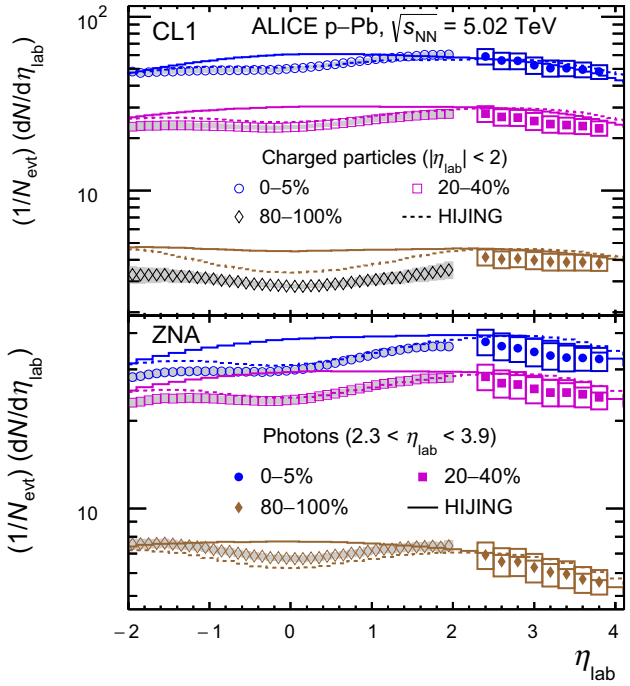

Fig. 10 Pseudorapidity distribution of inclusive photons measured within $2.3 < \eta_{lab} < 3.9$ in p–Pb collisions at $\sqrt{s_{NN}} = 5.02$ TeV compared with the charged-particle measurements [25] and to HIJING predictions for three centrality classes and for two centrality estimators: CL1 (top), ZNA (bottom)

the ZNA one. This could be attributed to the strong multiplicity bias as described in Ref. [25]. It is noted that the curve does not point towards the pp result. When the ZNA is used for the centrality estimation along with the hybrid method to determine the average number of participant nucleons ($N_{part}^{\text{high-}p_T}$ or $N_{part}^{\text{Pb-side}}$), the inclusive photon multiplicity is found to scale with $\langle N_{part}\rangle$ within uncertainties and to point towards the pp data point at low $\langle N_{part}\rangle$. Moreover, the range in $\langle N_{part}\rangle$ for the ZNA centrality selection is more limited (that could be because of saturation of forward neutron emission) than what is obtained by particle-multiplicity-based centrality estimators. This effect is also emphasized in Fig. 11(c) where the same quantity $\langle N_\gamma\rangle/\langle N_{part}\rangle$ is presented as a function of $\langle N_\gamma\rangle$. Similar results were observed for charged-particle multiplicity at midrapidity reported by ALICE in Ref. [25].

10 Summary

In summary, we have presented results for inclusive photon multiplicity and pseudorapidity distributions at forward rapidities ($2.3 < \eta_{lab} < 3.9$) in pp collisions at $\sqrt{s} = 5.02$ TeV and p–Pb and Pb–p collisions at $\sqrt{s_{NN}} = 5.02$ TeV. The centrality dependence of inclusive photon production is studied in p–Pb collisions for the CL1 and the ZNA centrality estimators. The evolution of the average photon multiplicity $\langle N_\gamma\rangle$ with $\sqrt{s}$ in pp collisions and with $\langle N_{part}\rangle$ in p–Pb collisions is presented. A comparison of inclusive photon production at forward rapidity with the production of charged particles at midrapidity is also discussed. The obtained results are compared to predictions from various event generators (PYTHIA 6 with the Perugia 2011 tune, PYTHIA 8 with the Monash 2013 tune, PHOJET, EPOS LHC for pp collisions and HIJING, DPMJET, AMPT for p–Pb and Pb–p collisions). The multiplicity distributions are well reproduced with double NBDs and results of the parameterization are provided.

The PYTHIA 8 generator with the Monash 2013 tune and the EPOS LHC generator do not reproduce the multiplicity distribution in pp collisions at high multiplicities whereas PYTHIA 6 with the Perugia 2011 tune and PHOJET better describe the data within uncertainties. For p–Pb collisions, none of the considered MC models could describe the multiplicity results in the full range. However, HIJING and AMPT are able to reproduce the tail of the distribution for both p–Pb and Pb–p collisions. Interestingly, compared to multiplicity distributions, the pseudorapidity distributions of inclusive photons are better described by all the considered MC models. The model predictions are found to describe the data within 20%. The pseudorapidity density of inclusive photons at forward rapidity follows the η_{lab} dependence of charged-particle multiplicity at midrapidity in pp and for various centrality classes in p–Pb collisions. This can be attributed to the fact that the major contribution to inclusive photons comes from the decay of neutral pions, and therefore the number of produced photons should be similar to that of charged particles. The models give similar pseudorapidity densities for photons and charged particles only at forward rapidity where the difference between η and y is negligible.

An asymmetric $dN_{ch}/d\eta_{lab}$ distribution for the asymmetric p–Pb collision system is evident for most central collisions while the distributions become more symmetric for the most peripheral class. HIJING describes the centrality evolution of both photon and charged-particle production within about 10–12%. The average photon multiplicity $\langle N_\gamma\rangle$ divided by the average number of participants scales linearly with both $N_{part}^{\text{high-}p_T}$ and $N_{part}^{\text{Pb-side}}$ estimated by the energy deposited in the ZDC and the trend with $\langle N_{part}\rangle$ is consistent with the data point from pp collisions at $\sqrt{s} = 5.02$ TeV.

These results of inclusive photon production in pp and p–Pb collisions provide important input for the tuning of theoretical models and MC event generators and help to establish the baseline measurements to interpret the Pb–Pb data.

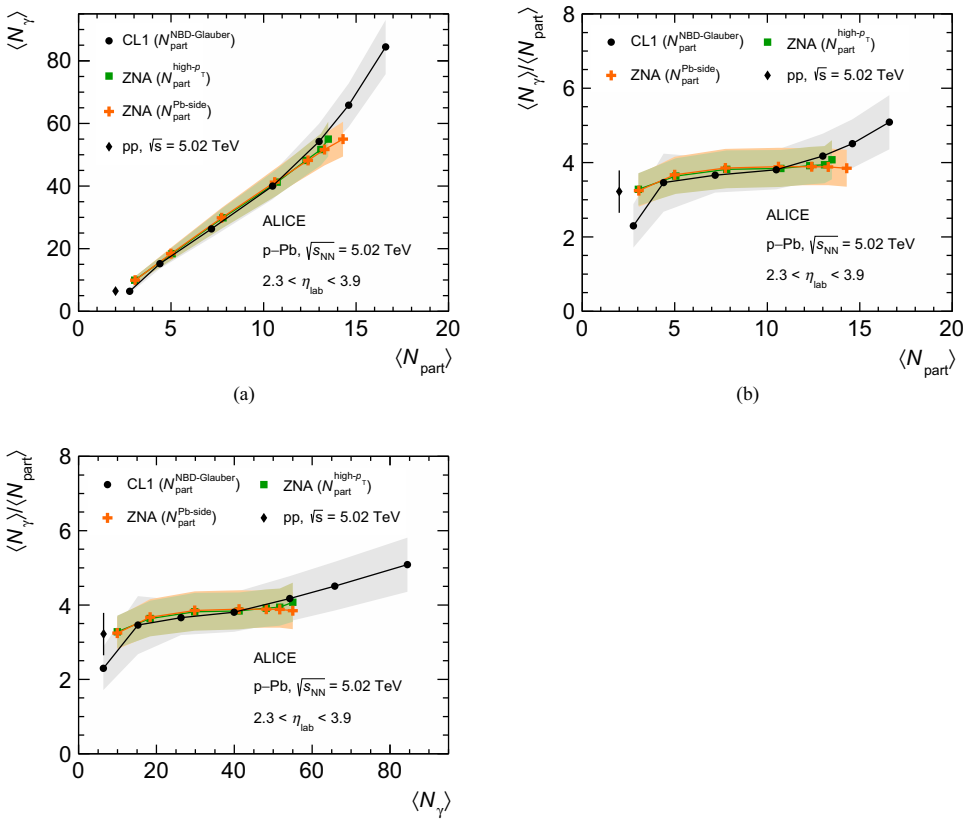

Fig. 11 (**a**) The average photon multiplicity $\langle N_\gamma \rangle$ within $2.3 < \eta_{lab} < 3.9$ as a function of the average number of participants for various centrality estimators in p–Pb collisions at $\sqrt{s_{NN}} = 5.02$ TeV. Values of $\langle N_\gamma \rangle / \langle N_{part} \rangle$ are shown as a function of $\langle N_{part} \rangle$ (**b**) and $\langle N_\gamma \rangle$ (**c**). The lines between the data points are to guide the eye. The data point for pp collisions at $\sqrt{s} = 5.02$ TeV is also included for reference

Table 7 The average photon multiplicity $\langle N_\gamma \rangle$ within $2.3 < \eta_{lab} < 3.9$ for various centrality classes defined using CL1 and ZNA centrality estimators in p–Pb collisions at $\sqrt{s_{NN}} = 5.02$ TeV. The corresponding values of $\langle N_{part} \rangle$ are taken from Ref. [25]. The quoted errors are systematic uncertainties. Statistical uncertainties are negligible

Centrality	CL1		ZNA		
	$\langle N_{part}^{NBD-Glauber} \rangle$	$\langle N_\gamma \rangle$	$\langle N_{part}^{high-p_T} \rangle$	$\langle N_{part}^{Pb-side} \rangle$	$\langle N_\gamma \rangle$
0–5%	16.60 ± 1.66	84.44 ± 8.65	13.50 ± 1.08	14.30 ± 1.14	54.98 ± 5.59
5–10%	14.60 ± 1.46	65.82 ± 6.96	13.10 ± 1.05	13.30 ± 1.06	51.65 ± 5.09
10–20%	13.00 ± 1.30	54.23 ± 5.67	12.30 ± 0.98	12.40 ± 0.99	48.18 ± 4.82
20–40%	10.49 ± 0.94	39.95 ± 4.22	10.73 ± 0.86	10.60 ± 0.85	41.22 ± 4.22
40–60%	7.18 ± 0.52	26.28 ± 2.79	7.81 ± 0.62	7.74 ± 0.62	29.82 ± 3.20
60–80%	4.40 ± 0.88	15.21 ± 1.60	5.05 ± 0.40	5.00 ± 0.40	18.36 ± 1.93
80–100%	2.76 ± 0.63	6.34 ± 0.68	3.03 ± 0.24	3.06 ± 0.24	9.93 ± 1.05

Acknowledgements The ALICE Collaboration would like to thank all its engineers and technicians for their invaluable contributions to the construction of the experiment and the CERN accelerator teams for the outstanding performance of the LHC complex. The ALICE Collaboration gratefully acknowledges the resources and support provided by all Grid centres and the Worldwide LHC Computing Grid (WLCG) collaboration. The ALICE Collaboration acknowledges the following funding agencies for their support in building and running the ALICE detector: A. I. Alikhanyan National Science Laboratory (Yerevan Physics Institute) Foundation (ANSL), State Committee of Science and World Federation of Scientists (WFS), Armenia; Austrian Academy of Sciences, Austrian Science Fund (FWF): [M 2467-N36] and Nationalstiftung für Forschung, Technologie und Entwicklung, Austria; Ministry of Communications and High Technologies, National Nuclear Research Center, Azerbaijan; Conselho Nacional de Desenvolvimento Científico e Tecnológico (CNPq), Financiadora de Estudos e Projetos (Finep), Fundação de Amparo à Pesquisa do Estado de São Paulo (FAPESP) and Universidade Federal do Rio Grande do Sul (UFRGS), Brazil; Bulgarian Ministry of Education and Science, within the National Roadmap for Research Infrastructures 2020-2027 (object CERN), Bulgaria; Ministry of Education of China (MOEC), Ministry of Science & Technology of China (MSTC) and National Natural Science Foundation of China (NSFC), China; Ministry of Science and Education and Croatian Science Foundation, Croatia; Centro de Aplicaciones Tecnológicas y Desarrollo Nuclear (CEADEN), Cubaenergía, Cuba; Ministry of Education, Youth and Sports of the Czech Republic, Czech Republic; The Danish Council for Independent Research | Natural Sciences, the VILLUM FONDEN and Danish National Research Foundation (DNRF), Denmark; Helsinki Institute of Physics (HIP), Finland; Commissariat à l'Energie Atomique (CEA) and

Institut National de Physique Nucléaire et de Physique des Particules (IN2P3) and Centre National de la Recherche Scientifique (CNRS), France; Bundesministerium für Bildung und Forschung (BMBF) and GSI Helmholtzzentrum für Schwerionenforschung GmbH, Germany; General Secretariat for Research and Technology, Ministry of Education, Research and Religions, Greece; National Research, Development and Innovation Office, Hungary; Department of Atomic Energy Government of India (DAE), Department of Science and Technology, Government of India (DST), University Grants Commission, Government of India (UGC) and Council of Scientific and Industrial Research (CSIR), India; National Research and Innovation Agency-BRIN, Indonesia; Istituto Nazionale di Fisica Nucleare (INFN), Italy; Japanese Ministry of Education, Culture, Sports, Science and Technology (MEXT) and Japan Society for the Promotion of Science (JSPS) KAKENHI, Japan; Consejo Nacional de Ciencia (CONACYT) y Tecnología, through Fondo de Cooperación Internacional en Ciencia y Tecnología (FONCICYT) and Dirección General de Asuntos del Personal Academico (DGAPA), Mexico; Nederlandse Organisatie voor Wetenschappelijk Onderzoek (NWO), Netherlands; The Research Council of Norway, Norway; Commission on Science and Technology for Sustainable Development in the South (COMSATS), Pakistan; Pontificia Universidad Católica del Perú, Peru; Ministry of Education and Science, National Science Centre and WUT ID-UB, Poland; Korea Institute of Science and Technology Information and National Research Foundation of Korea (NRF), Republic of Korea; Ministry of Education and Scientific Research, Institute of Atomic Physics, Ministry of Research and Innovation and Institute of Atomic Physics and University Politehnica of Bucharest, Romania; Ministry of Education, Science, Research and Sport of the Slovak Republic, Slovakia; National Research Foundation of South Africa, South Africa; Swedish Research Council (VR) and Knut & Alice Wallenberg Foundation (KAW), Sweden; European Organization for Nuclear Research, Switzerland; Suranaree University of Technology (SUT), National Science and Technology Development Agency (NSTDA), Thailand Science Research and Innovation (TSRI) and National Science, Research and Innovation Fund (NSRF), Thailand; Turkish Energy, Nuclear and Mineral Research Agency (TENMAK), Turkey; National Academy of Sciences of Ukraine, Ukraine; Science and Technology Facilities Council (STFC), United Kingdom; National Science Foundation of the United States of America (NSF) and United States Department of Energy, Office of Nuclear Physics (DOE NP), United States of America. In addition, individual groups or members have received support from: European Research Council, Strong 2020-Horizon 2020, Marie Skłodowska Curie (Grant Nos. 950692, 824093, 896850), European Union; Academy of Finland (Center of Excellence in Quark Matter) (Grant Nos. 346327, 346328), Finland; Programa de Apoyos para la Superación del Personal Académico, UNAM, Mexico.

Data Availability Statement This manuscript has no associated data or the data will not be deposited. [Authors' comment: Manuscript has associated data in the HEPData repository at https://www.hepdata.net/record/ins2637678.]

Funded by SCOAP^3. SCOAP^3 supports the goals of the International Year of Basic Sciences for Sustainable Development.

Appendix A

See Figs. 12 and 13.

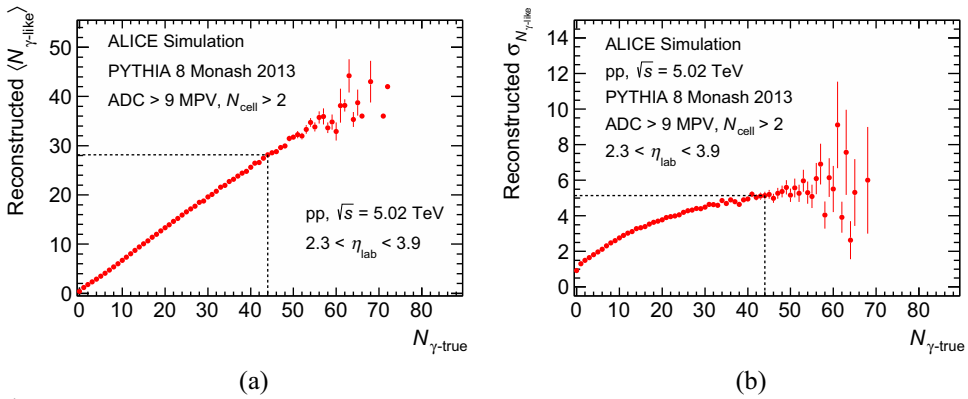

Fig. 12 The mean (**a**) and width (**b**) of the distribution of reconstructed photon multiplicity ($N_{\gamma\text{-like}}$) as a function of true photon multiplicity ($N_{\gamma\text{-true}}$) are presented for pp collisions at $\sqrt{s}$ = 5.02 TeV. The dotted lines correspond to $N_{\gamma\text{-true}}$ = 44 up to which the results are reported in the paper

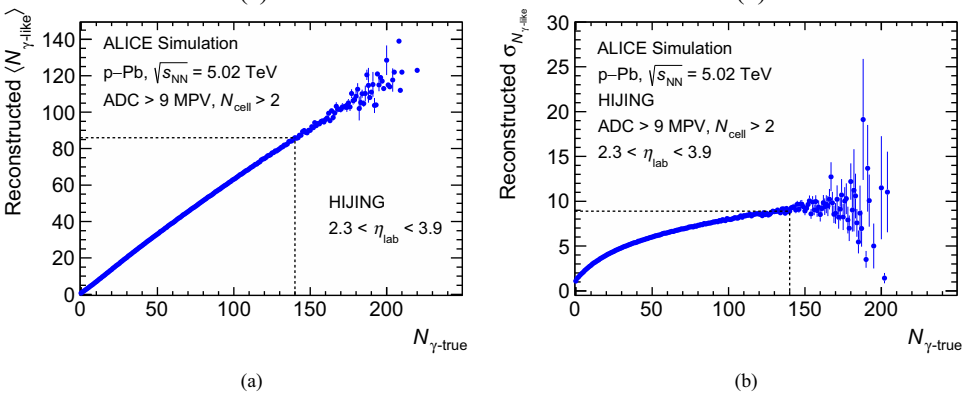

Fig. 13 The mean (**a**) and width (**b**) of the distribution of reconstructed photon multiplicity ($N_{\gamma\text{-like}}$) as a function of true photon multiplicity ($N_{\gamma\text{-true}}$) are presented for p–Pb collisions at $\sqrt{s_{NN}}$ = 5.02 TeV. The dotted lines correspond to $N_{\gamma\text{-true}}$ = 140 up to which the results are reported in the paper

References

1. P. Braun-Munzinger, V. Koch, T. Schäfer, J. Stachel, Properties of hot and dense matter from relativistic heavy-ion collisions. Phys. Rep. **621**, 76–126 (2016). https://doi.org/10.1016/j.physrep.2015.12.003. arXiv:1510.00442 [nucl-th]
2. J. Schukraft, Heavy Ion physics with the ALICE experiment at the CERN LHC. Philos. Trans. R. Soc. Lond. A **370**, 917–932 (2012). https://doi.org/10.1098/rsta.2011.0469. arXiv:1109.4291 [hep-ex]
3. **ALICE** Collaboration, The ALICE experiment—a journey through QCD. arXiv:2211.04384 [nucl-ex]
4. R. Xu, W.-T. Deng, X.-N. Wang, Nuclear modification of high-p_T hadron spectra in p-A collisions at LHC. Phys. Rev. C **86**, 051901 (2012). https://doi.org/10.1103/PhysRevC.86.051901. arXiv:1204.1998 [nucl-th]
5. M. Arneodo, Nuclear effects in structure functions. Phys. Rep. **240**, 301–393 (1994). https://doi.org/10.1016/0370-1573(94)90048-5
6. **CMS** Collaboration, V. Khachatryan et al., Observation of long-range near-side angular correlations in proton-proton collisions at the LHC. JHEP **09**, 091 (2010). https://doi.org/10.1007/JHEP09(2010)091. arXiv:1009.4122 [hep-ex]
7. **CMS** Collaboration, V. Khachatryan et al., Measurement of long-range near-side two-particle angular correlations in pp collisions at $\sqrt{s}$ =13 TeV. Phys. Rev. Lett. **116**, 172302 (2016). https://doi.org/10.1103/PhysRevLett.116.172302. arXiv:1510.03068 [nucl-ex]
8. **ATLAS** Collaboration, G. Aad et al., Observation of long-range elliptic azimuthal anisotropies in $\sqrt{s}$ =13 and 2.76 TeV pp collisions with the ATLAS detector. Phys. Rev. Lett.**116**, 172301 (2016). https://doi.org/10.1103/PhysRevLett.116.172301. arXiv:1509.04776 [hep-ex]
9. **ALICE** Collaboration, B. Abelev et al., Long-range angular correlations on the near and away side in p–Pb collisions at $\sqrt{s_{NN}}$ = 5.02 TeV. Phys. Lett. B **719**, 29–41 (2013). https://doi.org/10.1016/j.physletb.2013.01.012. arXiv:1212.2001 [nucl-ex]
10. **ATLAS** Collaboration, G. Aad et al., Observation of associated near-side and away-side long-range correlations in $\sqrt{s_{NN}}$ = 5.02 TeV p–Pb Collisions with the ATLAS detector. Phys. Rev. Lett. **110**, 182302 (2013). https://doi.org/10.1103/PhysRevLett.110.182302. arXiv:1212.5198 [hep-ex]
11. **CMS** Collaboration, S. Chatrchyan et al., Observation of long-range near-side angular correlations in p-Pb collisions at the LHC. Phys. Lett. B **718**, 795–814 (2013). https://doi.org/10.1016/j.physletb.2012.11.025. arXiv:1210.5482 [nucl-ex]
12. **ATLAS** Collaboration, G. Aad et al., Measurement of long-range pseudorapidity correlations and azimuthal harmonics in $\sqrt{s_{NN}}$ = 5.02 TeV p–Pb collisions with the ATLAS detector. Phys. Rev. C**90**, 044906 (2014). https://doi.org/10.1103/PhysRevC.90.044906. arXiv:1409.1792 [hep-ex]
13. **ALICE** Collaboration, J. Adam et al., Enhanced production of multi-strange hadrons in high-multiplicity proton–proton collisions. Nat. Phys. **13**, 535–539 (2017). https://doi.org/10.1038/nphys4111. arXiv:1606.07424 [nucl-ex]
14. D. Kharzeev, E. Levin, M. Nardi, Color glass condensate at the LHC: Hadron multiplicities in pp, p-A and A-A collisions. Nucl. Phys. A **747**, 609–629 (2005). https://doi.org/10.1016/j.nuclphysa.2004.10.018. arXiv:hep-ph/0408050
15. W.-T. Deng, X.-N. Wang, R. Xu, Hadron production in pp, p-Pb, and Pb-Pb collisions with the HIJING 2.0 model at energies available at the CERN Large Hadron Collider. Phys. Rev. C **83**, 014915 (2011). https://doi.org/10.1103/PhysRevC.83.014915. arXiv:1008.1841 [hep-ph]
16. **ALICE** Collaboration, B.B. Abelev et al., Inclusive photon production at forward rapidities in proton–proton collisions at $\sqrt{s}$ = 0.9, 2.76 and 7 TeV. Eur. Phys. J. C **75**, 146 (2015). https://doi.org/10.1140/epjc/s10052-015-3356-2. arXiv:1411.4981 [nucl-ex]
17. **STAR** Collaboration, J. Adams et al., Multiplicity and pseudorapidity distributions of photons in Au + Au collisions at $\sqrt{s_{NN}}$ = 62.4 GeV. Phys. Rev. Lett. **95**, 062301 (2005). https://doi.org/10.1103/PhysRevLett.95.062301. arXiv:nucl-ex/0502008

18. **STAR** Collaboration, J. Adams et al., Multiplicity and pseudorapidity distributions of charged particles and photons at forward pseudorapidity in Au + Au collisions at $\sqrt{s_{\rm NN}} = 62.4$ GeV. Phys. Rev. C **73**, 034906 (2006). https://doi.org/10.1103/PhysRevC.73.034906. arXiv:nucl-ex/0511026
19. **ALICE** Collaboration, K. Aamodt et al., First proton–proton collisions at the LHC as observed with the ALICE detector: measurement of the charged-particle pseudorapidity density at $\sqrt{s} = 900$ GeV. Eur. Phys. J. C **65**, 111–125 (2010). https://doi.org/10.1140/epjc/s10052-009-1227-4. arXiv:0911.5430 [hep-ex]
20. **ALICE** Collaboration, K. Aamodt et al., Charged-particle multiplicity measurement in proton–proton collisions at $\sqrt{s} = 0.9$ and 2.36 TeV with ALICE at LHC. Eur. Phys. J. C **68**, 89–108 (2010). https://doi.org/10.1140/epjc/s10052-010-1339-x. arXiv:1004.3034 [hep-ex]
21. **ALICE** Collaboration, K. Aamodt et al., Charged-particle multiplicity measurement in proton–proton collisions at $\sqrt{s} = 7$ TeV with ALICE at LHC. Eur. Phys. J. C**68**, 345–354 (2010). https://doi.org/10.1140/epjc/s10052-010-1350-2. arXiv:1004.3514 [hep-ex]
22. **ALICE** Collaboration, J. Adam et al., Charged-particle multiplicities in proton–proton collisions at $\sqrt{s} = 0.9$ to 8 TeV. Eur. Phys. J. C **77**, 33 (2017). https://doi.org/10.1140/epjc/s10052-016-4571-1. arXiv:1509.07541 [nucl-ex]
23. **ALICE** Collaboration, S. Acharya et al., Charged-particle multiplicity distributions over a wide pseudorapidity range in proton–proton collisions at $\sqrt{s} = 0.9$, 7, and 8 TeV. Eur. Phys. J. C **77**, 852 (2017). https://doi.org/10.1140/epjc/s10052-017-5412-6. arXiv:1708.01435 [hep-ex]
24. **ALICE** Collaboration, B. Abelev et al., Pseudorapidity density of charged particles in p–Pb collisions at $\sqrt{s_{\rm NN}} = 5.02$ TeV. Phys. Rev. Lett. **110**, 032301 (2013). https://doi.org/10.1103/PhysRevLett.110.032301. arXiv:1210.3615 [nucl-ex]
25. **ALICE** Collaboration, J. Adam et al., Centrality dependence of particle production in p–Pb collisions at $\sqrt{s_{\rm NN}} = 5.02$ TeV. Phys. Rev. C **91**, 064905 (2015). https://doi.org/10.1103/PhysRevC.91.064905. arXiv:1412.6828 [nucl-ex]
26. **ALICE** Collaboration, S. Acharya et al., Charged-particle pseudorapidity density at midrapidity in p–Pb collisions at $\sqrt{s_{\rm NN}} = 8.16$ TeV. Eur. Phys. J. C**79**, 307 (2019). https://doi.org/10.1140/epjc/s10052-019-6801-9. arXiv:1812.01312 [nucl-ex]
27. **ALICE** Collaboration, S. Acharya et al., Pseudorapidity distributions of charged particles as a function of mid- and forward rapidity multiplicities in pp collisions at $\sqrt{s} = 5.02$, 7 and 13 TeV. Eur. Phys. J. C **81**, 630 (2021). https://doi.org/10.1140/epjc/s10052-021-09349-5. arXiv:2009.09434 [nucl-ex]
28. **ALICE** Collaboration, K. Aamodt et al., Charged-particle multiplicity density at midrapidity in central Pb–Pb collisions at $\sqrt{s_{\rm NN}} = 2.76$ TeV. Phys. Rev. Lett. **105**, 252301 (2010). https://doi.org/10.1103/PhysRevLett.105.252301. arXiv:1011.3916 [nucl-ex]
29. **ALICE** Collaboration, K. Aamodt et al., Centrality dependence of the charged-particle multiplicity density at midrapidity in Pb–Pb collisions at $\sqrt{s_{\rm NN}} = 2.76$ TeV. Phys. Rev. Lett. **106**, 032301 (2011). https://doi.org/10.1103/PhysRevLett.106.032301. arXiv:1012.1657 [nucl-ex]
30. **ALICE** Collaboration, J. Adam et al., Centrality evolution of the charged-particle pseudorapidity density over a broad pseudorapidity range in Pb–Pb collisions at $\sqrt{s_{\rm NN}} = 2.76$ TeV. Phys. Lett. B **754**, 373–385 (2016). https://doi.org/10.1016/j.physletb.2015.12.082. arXiv:1509.07299 [nucl-ex]
31. **ALICE** Collaboration, E. Abbas et al., Centrality dependence of the pseudorapidity density distribution for charged particles in Pb–Pb collisions at $\sqrt{s_{\rm NN}} = 2.76$ TeV. Phys. Lett. B **726**, 610–622 (2013). https://doi.org/10.1016/j.physletb.2013.09.022. arXiv:1304.0347 [nucl-ex]
32. **ALICE** Collaboration, J. Adam et al., Centrality dependence of the charged-particle multiplicity density at midrapidity in Pb–Pb collisions at $\sqrt{s_{\rm NN}} = 5.02$ TeV. Phys. Rev. Lett. **116**, 222302 (2016). https://doi.org/10.1103/PhysRevLett.116.222302. arXiv:1512.06104 [nucl-ex]
33. **ALICE** Collaboration, J. Adam et al., Centrality dependence of the pseudorapidity density distribution for charged particles in Pb–Pb collisions at $\sqrt{s_{\rm NN}} = 5.02$ TeV. Phys. Lett. B **772**, 567–577 (2017). https://doi.org/10.1016/j.physletb.2017.07.017. arXiv:1612.08966 [nucl-ex]
34. **ATLAS** Collaboration, G. Aad et al., Charged-particle multiplicities in pp interactions at $\sqrt{s} = 900$ GeV measured with the ATLAS detector at the LHC. Phys. Lett. B **688**, 21–42 (2010). https://doi.org/10.1016/j.physletb.2010.03.064. arXiv:1003.3124 [hep-ex]
35. **ATLAS** Collaboration, G. Aad et al., Charged-particle multiplicities in pp interactions measured with the ATLAS detector at the LHC. New J. Phys. **13**, 053033 (2011). https://doi.org/10.1088/1367-2630/13/5/053033. arXiv:1012.5104 [hep-ex]
36. **ATLAS** Collaboration, G. Aad et al., Charged-particle distributions in pp interactions at $\sqrt{s} = 8$ TeV measured with the ATLAS detector. Eur. Phys. J. C **76**, 403 (2016). https://doi.org/10.1140/epjc/s10052-016-4203-9. arXiv:1603.02439 [hep-ex]
37. **ATLAS** Collaboration, G. Aad et al., Measurement of the centrality dependence of the charged-particle pseudorapidity distribution in p–Pb collisions at $\sqrt{s_{\rm NN}} = 5.02$ TeV with the ATLAS detector. Eur. Phys. J. C **76**, 199 (2016). https://doi.org/10.1140/epjc/s10052-016-4002-3. arXiv:1508.00848 [hep-ex]
38. **ATLAS** Collaboration, G. Aad et al., Measurement of the centrality dependence of the charged-particle pseudorapidity distribution in Pb–Pb collisions at $\sqrt{s_{\rm NN}} = 2.76$ TeV with the ATLAS detector. Phys. Lett. B **710**, 363–382 (2012). https://doi.org/10.1016/j.physletb.2012.02.045. arXiv:1108.6027 [hep-ex]
39. **CMS** Collaboration, V. Khachatryan et al., Charged-particle multiplicities in pp interactions at $\sqrt{s} = 0.9$, 2.36, and 7 TeV. JHEP **01**, 079 (2011). https://doi.org/10.1007/JHEP01(2011)079. arXiv:1011.5531 [hep-ex]
40. **CMS** Collaboration, V. Khachatryan et al., Pseudorapidity distribution of charged hadrons in proton-proton collisions at $\sqrt{s} = 13$ TeV. Phys. Lett. B **751**, 143–163 (2015). https://doi.org/10.1016/j.physletb.2015.10.004. arXiv:1507.05915 [hep-ex]
41. **CMS** Collaboration, A.M. Sirunyan et al., Pseudorapidity distributions of charged hadrons in p–Pb collisions at $\sqrt{s_{\rm NN}} = 5.02$ and 8.16 TeV. JHEP **01**, 045 (2018). https://doi.org/10.1007/JHEP01(2018)045. arXiv:1710.09355 [hep-ex]
42. **CMS** Collaboration, S. Chatrchyan et al., Dependence on pseudorapidity and centrality of charged hadron production in Pb–Pb collisions at $\sqrt{s_{\rm NN}} = 2.76$ TeV. JHEP **08**, 141 (2011). https://doi.org/10.1007/JHEP08(2011)141. arXiv:1107.4800 [nucl-ex]
43. **LHCb** Collaboration, R. Aaij et al., Measurement of charged-particle multiplicities and densities in pp collisions at $\sqrt{s} = 7$ TeV in the forward region. Eur. Phys. J. C **74**, 2888 (2014). https://doi.org/10.1140/epjc/s10052-014-2888-1. arXiv:1402.4430 [hep-ex]
44. **ALICE** Collaboration, K. Aamodt et al., The ALICE experiment at the CERN LHC. JINST **3**, S08002 (2008). https://doi.org/10.1088/1748-0221/3/08/S08002
45. **ALICE** Collaboration, B.B. Abelev et al., Performance of the ALICE experiment at the CERN LHC. Int. J. Mod. Phys. A **29**, 1430044 (2014). https://doi.org/10.1142/S0217751X14300440. arXiv:1402.4476 [nucl-ex]
46. **ALICE** Collaboration, G. Dellacasa et al., ALICE technical design report: Photon multiplicity detector (PMD). CERN-LHCC-99-032. http://cds.cern.ch/record/451099
47. **ALICE** Collaboration, P. Cortese et al., ALICE: addendum to the technical design report of the photon multiplicity detector (PMD). CERN-LHCC-2003-038. https://cds.cern.ch/record/642177

48. **ALICE** Collaboration, K. Aamodt et al., Alignment of the ALICE Inner Tracking System with cosmic-ray tracks. JINST **5**, P03003 (2010). https://doi.org/10.1088/1748-0221/5/03/P03003. arXiv:1001.0502 [physics.ins-det]
49. **ALICE** Collaboration, P. Cortese et al., ALICE forward detectors: FMD, TO and VO: Technical Design Report. CERN-LHCC-2004-025. https://cds.cern.ch/record/781854
50. **ALICE** Collaboration, E. Abbas et al., Performance of the ALICE VZERO system. JINST **8**, P10016 (2013). https://doi.org/10.1088/1748-0221/8/10/P10016. arXiv:1306.3130 [nucl-ex]
51. **ALICE** Collaboration, M. Gallio, W. Klempt, L. Leistam, J. De Groot, J. Schukraft, ALICE Zero Degree Calorimeter (ZDC): Technical Design Report. CERN-LHCC-99-005. https://cds.cern.ch/record/381433
52. **ALICE** Collaboration, L. Betev et al., Definition of the ALICE coordinate system and basic rules for sub-detector components numbering. https://edms.cern.ch/ui/#!master/navigator/document?D:1020137949:1020137949:subDocs
53. M.L. Miller, K. Reygers, S.J. Sanders, P. Steinberg, Glauber modeling in high energy nuclear collisions. Ann. Rev. Nucl. Part. Sci. **57**, 205–243 (2007). https://doi.org/10.1146/annurev.nucl.57.090506.123020. arXiv:nucl-ex/0701025
54. D. d'Enterria, C. Loizides, Progress in the Glauber model at collider energies. Ann. Rev. Nucl. Part. Sci. **71**, 315–344 (2021). https://doi.org/10.1146/annurev-nucl-102419-060007. arXiv:2011.14909 [hep-ph]
55. F. Sikler, Centrality control of hadron nucleus interactions by detection of slow nucleons. arXiv:hep-ph/0304065
56. B. Alessandro et al., ALICE: physics performance report, volume II. J. Phys. G Nucl. Part. Phys. **32**, 1295–2040 (2006). https://doi.org/10.1088/0954-3899/32/10/001
57. X.-N. Wang, M. Gyulassy, HIJING: a Monte Carlo model for multiple jet production in pp, p-A and A-A collisions. Phys. Rev. D **44**, 3501–3516 (1991). https://doi.org/10.1103/PhysRevD.44.3501
58. S. Roesler, R. Engel, J. Ranft, The Monte Carlo event generator DPMJET-III, in *International Conference on Advanced Monte Carlo for Radiation Physics, Particle Transport Simulation and Applications (MC 2000)*, vol. 12, pp. 1033–1038 (2000). https://doi.org/10.1007/978-3-642-18211-2_166. arXiv:hep-ph/0012252 [hep-ph]
59. P. Skands, S. Carrazza, J. Rojo, Tuning PYTHIA 8.1: the Monash 2013 Tune. Eur. Phys. J. C **74**, 3024 (2014). https://doi.org/10.1140/epjc/s10052-014-3024-y. arXiv:1404.5630 [hep-ph]
60. T. Pierog et al., EPOS LHC: test of collective hadronization with data measured at the CERN Large Hadron Collider. Phys. Rev. C **92**, 034906 (2015). https://doi.org/10.1103/PhysRevC.92.034906. arXiv:1306.0121 [hep-ph]
61. R. Brun et al., GEANT: Detector Description and Simulation Tool. CERN Program Library. CERN, Geneva (1993). https://doi.org/10.17181/CERN.MUHF.DMJ1http://cds.cern.ch/record/1082634
62. R. Brun et al., Computing in ALICE. Nucl. Instrum. Methods A **502**, 339–346 (2003). https://doi.org/10.1016/S0168-9002(03)00440-6
63. C. Bierlich et al., A comprehensive guide to the physics and usage of PYTHIA 8.3. arXiv:2203.11601 [hep-ph]
64. T. Sjöstrand, M. van Zijl, A multiple-interaction model for the event structure in hadron collisions. Phys. Rev. D **36**, 2019–2041 (1987). https://doi.org/10.1103/PhysRevD.36.2019
65. T. Sjöstrand et al., An introduction to PYTHIA 8.2. Comput. Phys. Commun. **191**, 159–177 (2015). https://doi.org/10.1016/j.cpc.2015.01.024. arXiv:1410.3012 [hep-ph]
66. J.R. Christiansen, P.Z. Skands, String formation beyond leading colour. JHEP **08**, 003 (2015). https://doi.org/10.1007/JHEP08(2015)003. arXiv:1505.01681 [hep-ph]
67. H. Pi, An event generator for interactions between hadrons and nuclei: FRITIOF version 7.0. Comput. Phys. Commun. **71**, 173–192 (1992). https://doi.org/10.1016/0010-4655(92)90082-A
68. A. Capella, U. Sukhatme, C. I. Tan, J. Tran Thanh Van, Dual parton model. Phys. Rep. **236**, 225–329 (1994) https://doi.org/10.1016/0370-1573(94)90064-7
69. P.D.B. Collins, An introduction to Regge theory and high-energy physics. Cambridge Monographs on Mathematical Physics. Cambridge Univ. Press, Cambridge, p 5 (2009). https://doi.org/10.1017/CBO9780511897603
70. **CDF** Collaboration, F. Abe et al., Measurement of $p\bar{p}$ single diffraction dissociation at $\sqrt{s} = 546$ GeV and 1800 GeV. Phys. Rev. D **50**, 5535–5549 (1994). https://doi.org/10.1103/PhysRevD.50.5535
71. **CDF** Collaboration, F. Abe et al., Observation of rapidity gaps in $p\bar{p}$ collisions at 1.8 TeV. Phys. Rev. Lett. **74**, 855–859 (1995). https://doi.org/10.1103/PhysRevLett.74.855
72. **ALICE** Collaboration, B. Abelev et al., Measurement of inelastic, single- and double-diffraction cross sections in proton–proton collisions at the LHC with ALICE. Eur. Phys. J. C **73**, 2456 (2013). https://doi.org/10.1140/epjc/s10052-013-2456-0. arXiv:1208.4968 [hep-ex]
73. G. D'Agostini, A multidimensional unfolding method based on Bayes' theorem. Nucl. Instrum. Methods Phys. Res. Sect. A **362**, 487–498 (1995). https://doi.org/10.1016/0168-9002(95)00274-X
74. T. Adye, Unfolding algorithms and tests using RooUnfold. arXiv:1105.1160 [physics.data-an]
75. A. Hocker, V. Kartvelishvili, SVD approach to data unfolding. Nucl. Instrum. Methods A **372**, 469–481 (1996). https://doi.org/10.1016/0168-9002(95)01478-0. arXiv:hep-ph/9509307
76. P.Z. Skands, Tuning Monte Carlo generators: the Perugia tunes. Phys. Rev. D **82**, 074018 (2010). https://doi.org/10.1103/PhysRevD.82.074018. arXiv:1005.3457 [hep-ph]
77. F.W. Bopp, R. Engel, J. Ranft, Rapidity gaps and the PHOJET Monte Carlo, in *LAFEX International School on High-Energy Physics (LISHEP 98) Session A: Particle Physics for High School Teachers—Session B: Advanced School in HEP—Session C: Workshop on Diffractive Physics*, vol. 3, pp. 729–741 (1998). arXiv:hep-ph/9803437
78. Z.-W. Lin, C.M. Ko, B.-A. Li, B. Zhang, S. Pal, Multiphase transport model for relativistic heavy-ion collisions. Phys. Rev. C **72**, 064901 (2005). https://doi.org/10.1103/PhysRevC.72.064901. arXiv:nucl-th/0411110
79. **ALICE** Collaboration, Pseudorapidity densities of charged particles with transverse momentum thresholds in pp collisions at $\sqrt{s} = 5.02$ and 13 TeV. arXiv:2211.15364 [nucl-ex]

ALICE Collaboration*

S. Acharya[125], D. Adamová[86], A. Adler[69], G. Aglieri Rinella[32], M. Agnello[29], N. Agrawal[50], Z. Ahammed[132], S. Ahmad[15], S. U. Ahn[70], I. Ahuja[37], A. Akindinov[140], M. Al-Turany[97], D. Aleksandrov[140], B. Alessandro[55], H. M. Alfanda[6], R. Alfaro Molina[66], B. Ali[15], A. Alici[25], N. Alizadehvandchali[114], A. Alkin[32], J. Alme[20], G. Alocco[51], T. Alt[63], I. Altsybeev[140], M. N. Anaam[6], C. Andrei[45], A. Andronic[135], V. Anguelov[94], F. Antinori[53], P. Antonioli[50], N. Apadula[74], L. Aphecetche[103], H. Appelshäuser[63], C. Arata[73], S. Arcelli[25], M. Aresti[51], R. Arnaldi[55], J. G. M. C. A. Arneiro[110], I. C. Arsene[19], M. Arslandok[137], A. Augustinus[32], R. Averbeck[97], M. D. Azmi[15], A. Badalà[52], J. Bae[104], Y. W. Baek[40], X. Bai[118], R. Bailhache[63], Y. Bailung[47], A. Balbino[29], A. Baldisseri[128], B. Balis[2], D. Banerjee[4], Z. Banoo[91], R. Barbera[26], F. Barile[31], L. Barioglio[95], M. Barlou[78], G. G. Barnaföldi[136], L. S. Barnby[85], V. Barret[125], L. Barreto[110], C. Bartels[117], K. Barth[32], E. Bartsch[63], N. Bastid[125], S. Basu[75], G. Batigne[103], D. Battistini[95], B. Batyunya[141], D. Bauri[46], J. L. Bazo Alba[101], I. G. Bearden[83], C. Beattie[137], P. Becht[97], D. Behera[47], I. Belikov[127], A. D. C. Bell Hechavarria[135], F. Bellini[25], R. Bellwied[114], S. Belokurova[140], V. Belyaev[140], G. Bencedi[136], S. Beole[24], A. Bercuci[45], Y. Berdnikov[140], A. Berdnikova[94], L. Bergmann[94], M. G. Besoiu[62], L. Betev[32], P. P. Bhaduri[132], A. Bhasin[91], M. A. Bhat[4], B. Bhattacharjee[41], L. Bianchi[24], N. Bianchi[48], J. Bielčík[35], J. Bielčíková[86], J. Biernat[107], A. P. Bigot[127], A. Bilandzic[95], G. Biro[136], S. Biswas[4], N. Bize[103], J. T. Blair[108], D. Blau[140], M. B. Blidaru[97], N. Bluhme[38], C. Blume[63], G. Boca[21,54], F. Bock[87], T. Bodova[20], A. Bogdanov[140], S. Boi[22], J. Bok[57], L. Boldizsár[136], M. Bombara[37], P. M. Bond[32], G. Bonomi[54,131], H. Borel[128], A. Borissov[140], A. G. Borquez Carcamo[94], H. Bossi[137], E. Botta[24], Y. E. M. Bouziani[63], L. Bratrud[63], P. Braun-Munzinger[97], M. Bregant[110], M. Broz[35], G. E. Bruno[31,96], M. D. Buckland[23], D. Budnikov[140], H. Buesching[63], S. Bufalino[29], P. Buhler[102], Z. Buthelezi[67,121], A. Bylinkin[20], S. A. Bysiak[107], M. Cai[6], H. Caines[137], A. Caliva[97], E. Calvo Villar[101], J. M. M. Camacho[109], P. Camerini[23], F. D. M. Canedo[110], M. Carabas[124], A. A. Carballo[32], F. Carnesecchi[32], R. Caron[126], L. A. D. Carvalho[110], J. Castillo Castellanos[128], F. Catalano[24,32], C. Ceballos Sanchez[141], I. Chakaberia[74], P. Chakraborty[46], S. Chandra[132], S. Chapeland[32], M. Chartier[117], S. Chattopadhyay[132], S. Chattopadhyay[99], T. G. Chavez[44], T. Cheng[6,97], C. Cheshkov[126], B. Cheynis[126], V. Chibante Barroso[32], D. D. Chinellato[111], E. S. Chizzali[95,a], J. Cho[57], S. Cho[57], P. Chochula[32], P. Christakoglou[84], C. H. Christensen[83], P. Christiansen[75], T. Chujo[123], M. Ciacco[29], C. Cicalo[51], F. Cindolo[50], M. R. Ciupek[97], G. Clai[50,b], F. Colamaria[49], J. S. Colburn[100], D. Colella[31,96], M. Colocci[25], G. Conesa Balbastre[73], Z. Conesa del Valle[72], G. Contin[23], J. G. Contreras[35], M. L. Coquet[128], T. M. Cormier[87,f], P. Cortese[55,130], M. R. Cosentino[112], F. Costa[32], S. Costanza[21,54], C. Cot[72], J. Crkovská[94], P. Crochet[125], R. Cruz-Torres[74], P. Cui[6], A. Dainese[53], M. C. Danisch[94], A. Danu[62], P. Das[80], P. Das[4], S. Das[4], A. R. Dash[135], S. Dash[46], R. M. H. David[44], S. De[80], A. De Caro[28], G. de Cataldo[49], J. de Cuveland[38], A. De Falco[22], D. De Gruttola[28], N. De Marco[55], C. De Martin[23], S. De Pasquale[28], R. Deb[131], S. Deb[47], R. J. Debski[2], K. R. Deja[133], R. Del Grande[95], L. Dello Stritto[28], W. Deng[6], P. Dhankher[18], D. Di Bari[31], A. Di Mauro[32], R. A. Diaz[7,141], T. Dietel[113], Y. Ding[6], R. Divià[32], D. U. Dixit[18], Ø. Djuvsland[20], U. Dmitrieva[140], A. Dobrin[62], B. Dönigus[63], J. M. Dubinski[133], A. Dubla[97], S. Dudi[90], P. Dupieux[125], M. Durkac[106], N. Dzalaiova[12], T. M. Eder[135], R. J. Ehlers[74], F. Eisenhut[63], D. Elia[49], B. Erazmus[103], F. Ercolessi[25], F. Erhardt[89], M. R. Ersdal[20], B. Espagnon[72], G. Eulisse[32], D. Evans[100], S. Evdokimov[140], L. Fabbietti[95], M. Faggin[27], J. Faivre[73], F. Fan[6], W. Fan[74], A. Fantoni[48], M. Fasel[87], P. Fecchio[29], A. Feliciello[55], G. Feofilov[140], A. Fernández Téllez[44], L. Ferrandi[110], M. B. Ferrer[32], A. Ferrero[128], C. Ferrero[55], A. Ferretti[24], V. J. G. Feuillard[94], V. Filova[35], D. Finogeev[140], F. M. Fionda[51], F. Flor[114], A. N. Flores[108], S. Foertsch[67], I. Fokin[94], S. Fokin[140], E. Fragiacomo[56], E. Frajna[136], U. Fuchs[32], N. Funicello[28], C. Furget[73], A. Furs[140], T. Fusayasu[98], J. J. Gaardhøje[83], M. Gagliardi[24], A. M. Gago[101], C. D. Galvan[109], D. R. Gangadharan[114], P. Ganoti[78], C. Garabatos[97], J. R. A. Garcia[44], E. Garcia-Solis[9], C. Gargiulo[32], K. Garner[135], P. Gasik[97], A. Gautam[116], M. B. Gay Ducati[65], M. Germain[103], A. Ghimouz[123], C. Ghosh[132], M. Giacalone[25,50], P. Giubellino[55,97], P. Giubilato[27], A. M. C. Glaenzer[128], P. Glässel[94], E. Glimos[120], D. J. Q. Goh[76], V. Gonzalez[134], M. Gorgon[2], S. Gotovac[33], V. Grabski[66], L. K. Graczykowski[133], E. Grecka[86], A. Grelli[58], C. Grigoras[32], V. Grigoriev[140], S. Grigoryan[1,141], F. Grosa[32], J. F. Grosse-Oetringhaus[32], R. Grosso[97], D. Grund[35], G. G. Guardiano[111], R. Guernane[73], M. Guilbaud[103], K. Gulbrandsen[83], T. Gundem[63], T. Gunji[122], W. Guo[6], A. Gupta[91], R. Gupta[91], R. Gupta[47], S. P. Guzman[44], K. Gwizdziel[133], L. Gyulai[136], M. K. Habib[97], C. Hadjidakis[72], F. U. Haider[91], H. Hamagaki[76], A. Hamdi[74], M. Hamid[6],

Y. Han[138], R. Hannigan[108], J. Hansen[75], M. R. Haque[133], J. W. Harris[137], A. Harton[9], H. Hassan[87], D. Hatzifotiadou[50], P. Hauer[42], L. B. Havener[137], S. T. Heckel[95], E. Hellbär[97], H. Helstrup[34], M. Hemmer[63], T. Herman[35], G. Herrera Corral[8], F. Herrmann[135], S. Herrmann[126], K. F. Hetland[34], B. Heybeck[63], H. Hillemanns[32], B. Hippolyte[127], F. W. Hoffmann[69], B. Hofman[58], B. Hohlweger[84], G. H. Hong[138], M. Horst[95], A. Horzyk[2], Y. Hou[6], P. Hristov[32], C. Hughes[120], P. Huhn[63], L. M. Huhta[115], T. J. Humanic[88], A. Hutson[114], D. Hutter[38], R. Ilkaev[140], H. Ilyas[13], M. Inaba[123], G. M. Innocenti[32], M. Ippolitov[140], A. Isakov[86], T. Isidori[116], M. S. Islam[99], M. Ivanov[12], M. Ivanov[97], V. Ivanov[140], M. Jablonski[2], B. Jacak[74], N. Jacazio[32], P. M. Jacobs[74], S. Jadlovska[106], J. Jadlovsky[106], S. Jaelani[82], C. Jahnke[111], M. J. Jakubowska[133], M. A. Janik[133], T. Janson[69], M. Jercic[89], S. Jia[10], A. A. P. Jimenez[64], F. Jonas[87], J. M. Jowett[32,97], J. Jung[63], M. Jung[63], A. Junique[32], A. Jusko[100], M. J. Kabus[32,133], J. Kaewjai[105], P. Kalinak[59], A. S. Kalteyer[97], A. Kalweit[32], V. Kaplin[140], A. Karasu Uysal[71], D. Karatovic[89], O. Karavichev[140], T. Karavicheva[140], P. Karczmarczyk[133], E. Karpechev[140], U. Kebschull[69], R. Keidel[139], D. L. D. Keijdener[58], M. Keil[32], B. Ketzer[42], S. S. Khade[47], A. M. Khan[6,118], S. Khan[15], A. Khanzadeev[140], Y. Kharlov[140], A. Khatun[15,116], A. Khuntia[107], M. B. Kidson[113], B. Kileng[34], B. Kim[104], C. Kim[16], D. J. Kim[115], E. J. Kim[68], J. Kim[138], J. S. Kim[40], J. Kim[68], M. Kim[18], S. Kim[17], T. Kim[138], K. Kimura[92], S. Kirsch[63], I. Kisel[38], S. Kiselev[140], A. Kisiel[133], J. P. Kitowski[2], J. L. Klay[5], J. Klein[32], S. Klein[74], C. Klein-Bösing[135], M. Kleiner[63], T. Klemenz[95], A. Kluge[32], A. G. Knospe[114], C. Kobdaj[105], T. Kollegger[97], A. Kondratyev[141], N. Kondratyeva[140], E. Kondratyuk[140], J. Konig[63], S. A. Konigstorfer[95], P. J. Konopka[32], G. Kornakov[133], S. D. Koryciak[2], A. Kotliarov[86], V. Kovalenko[140], M. Kowalski[107], V. Kozhuharov[36], I. Králik[59], A. Kravčáková[37], L. Krcal[32,38], M. Krivda[59,100], F. Krizek[86], K. Krizkova Gajdosova[32], M. Kroesen[94], M. Krüger[63], D. M. Krupova[35], E. Kryshen[140], V. Kučera[57], C. Kuhn[127], P. G. Kuijer[84], T. Kumaoka[123], D. Kumar[132], L. Kumar[90], N. Kumar[90], S. Kumar[31], S. Kundu[32], P. Kurashvili[79], A. Kurepin[140], A. B. Kurepin[140], A. Kuryakin[140], S. Kushpil[86], J. Kvapil[100], M. J. Kweon[57], J. Y. Kwon[57], Y. Kwon[138], S. L. La Pointe[38], P. La Rocca[26], A. Lakrathok[105], M. Lamanna[32], R. Langoy[119], P. Larionov[32], E. Laudi[32], L. Lautner[32,95], R. Lavicka[102], T. Lazareva[140], R. Lea[54,131], H. Lee[104], I. Legrand[45], G. Legras[135], J. Lehrbach[38], T. M. Lelek[2], R. C. Lemmon[85], I. León Monzón[109], M. M. Lesch[95], E. D. Lesser[18], P. Lévai[136], X. Li[10], X. L. Li[6], J. Lien[119], R. Lietava[100], I. Likmeta[114], B. Lim[24], S. H. Lim[16], V. Lindenstruth[38], A. Lindner[45], C. Lippmann[97], A. Liu[18], D. H. Liu[6], J. Liu[117], I. M. Lofnes[20], C. Loizides[87], S. Lokos[107], J. Lomker[58], P. Loncar[33], J. A. Lopez[94], X. Lopez[125], E. López Torres[7], P. Lu[97,118], J. R. Luhder[135], M. Lunardon[27], G. Luparello[56], Y. G. Ma[39], A. Maevskaya[140], M. Mager[32], A. Maire[127], M. V. Makariev[36], M. Malaev[140], G. Malfattore[25], N. M. Malik[91], Q. W. Malik[19], S. K. Malik[91], L. Malinina[141,e], D. Mal'Kevich[140], D. Mallick[80], N. Mallick[47], G. Mandaglio[30,52], S. K. Mandal[79], V. Manko[140], F. Manso[125], V. Manzari[49], Y. Mao[6], G. V. Margagliotti[23], A. Margotti[50], A. Marín[97], C. Markert[108], P. Martinengo[32], J. L. Martinez[114], M. I. Martínez[44], G. Martínez García[103], M. P. P. Martins[110], S. Masciocchi[97], M. Masera[24], A. Masoni[51], L. Massacrier[72], A. Mastroserio[49,129], O. Matonoha[75], P. F. T. Matuoka[110], A. Matyja[107], C. Mayer[107], A. L. Mazuecos[32], F. Mazzaschi[24], M. Mazzilli[32], J. E. Mdhluli[121], A. F. Mechler[63], Y. Melikyan[43,140], A. Menchaca-Rocha[66], E. Meninno[28,102], A. S. Menon[114], M. Meres[12], S. Mhlanga[67,113], Y. Miake[123], L. Micheletti[55], L. C. Migliorin[126], D. L. Mihaylov[95], K. Mikhaylov[140,141], A. N. Mishra[136], D. Miśkowiec[97], A. Modak[4], A. P. Mohanty[58], B. Mohanty[80], M. Mohisin Khan[15,c], M. A. Molander[43], Z. Moravcova[83], C. Mordasini[95], D. A. Moreira De Godoy[135], I. Morozov[140], A. Morsch[32], T. Mrnjavac[32], V. Muccifora[48], S. Muhuri[132], J. D. Mulligan[74], A. Mulliri[22], M. G. Munhoz[110], R. H. Munzer[63], H. Murakami[122], S. Murray[113], L. Musa[32], J. Musinsky[59], J. W. Myrcha[133], B. Naik[121], A. I. Nambrath[18], B. K. Nandi[46], R. Nania[50], E. Nappi[49], A. F. Nassirpour[17,75], A. Nath[94], C. Nattrass[120], T. K. Nayak[80], M. N. Naydenov[36], A. Neagu[19], A. Negru[124], L. Nellen[64], S. V. Nesbo[34], G. Neskovic[38], D. Nesterov[140], B. S. Nielsen[83], E. G. Nielsen[83], S. Nikolaev[140], S. Nikulin[140], V. Nikulin[140], F. Noferini[50], S. Noh[11], P. Nomokonov[141], J. Norman[117], N. Novitzky[123], P. Nowakowski[133], A. Nyanin[140], J. Nystrand[20], M. Ogino[76], A. Ohlson[75], V. A. Okorokov[140], J. Oleniacz[133], A. C. Oliveira Da Silva[120], M. H. Oliver[137], A. Onnerstad[115], C. Oppedisano[55], A. Ortiz Velasquez[64], J. Otwinowski[107], M. Oya[92], K. Oyama[76], Y. Pachmayer[94], S. Padhan[46], D. Pagano[54,131], G. Paić[64], A. Palasciano[49], S. Panebianco[128], H. Park[123], H. Park[104], J. Park[57], J. E. Parkkila[32], R. N. Patra[91], B. Paul[22], H. Pei[6], T. Peitzmann[58], X. Peng[6], M. Pennisi[24], L. G. Pereira[65], D. Peresunko[140], G. M. Perez[7], S. Perrin[128], Y. Pestov[140], V. Petráček[35], V. Petrov[140], M. Petrovici[45], R. P. Pezzi[65,103], S. Piano[56], M. Pikna[12], P. Pillot[103], O. Pinazza[32,50], L. Pinsky[114], C. Pinto[95], S. Pisano[48], M. Płoskoń[74],

M. Planinic[89], F. Pliquett[63], M. G. Poghosyan[87], B. Polichtchouk[140], S. Politano[29], N. Poljak[89], A. Pop[45], S. Porteboeuf-Houssais[125], V. Pozdniakov[141], I. Y. Pozos[44], K. K. Pradhan[47], S. K. Prasad[4], S. Prasad[47], R. Preghenella[50], F. Prino[55], C. A. Pruneau[134], I. Pshenichnov[140], M. Puccio[32], S. Pucillo[24], Z. Pugelova[106], S. Qiu[84], L. Quaglia[24], R. E. Quishpe[114], S. Ragoni[14], A. Rakotozafindrabe[128], L. Ramello[55,130], F. Rami[127], S. A. R. Ramirez[44], T. A. Rancien[73], M. Rasa[26], S. S. Räsänen[43], R. Rath[50], M. P. Rauch[20], I. Ravasenga[84], K. F. Read[87,120], C. Reckziegel[112], A. R. Redelbach[38], K. Redlich[79,d], C. A. Reetz[97], A. Rehman[20], F. Reidt[32], H. A. Reme-Ness[34], Z. Rescakova[37], K. Reygers[94], A. Riabov[140], V. Riabov[140], R. Ricci[28], M. Richter[19], A. A. Riedel[95], W. Riegler[32], C. Ristea[62], M. Rodríguez Cahuantzi[44], K. Røed[19], R. Rogalev[140], E. Rogochaya[141], T. S. Rogoschinski[63], D. Rohr[32], D. Röhrich[20], P. F. Rojas[44], S. Rojas Torres[35], P. S. Rokita[133], G. Romanenko[141], F. Ronchetti[48], A. Rosano[30,52], E. D. Rosas[64], K. Roslon[133], A. Rossi[53], A. Roy[47], S. Roy[46], N. Rubini[25], O. V. Rueda[114], D. Ruggiano[133], R. Rui[23], P. G. Russek[2], R. Russo[84], A. Rustamov[81], E. Ryabinkin[140], Y. Ryabov[140], A. Rybicki[107], H. Rytkonen[115], W. Rzesa[133], O. A. M. Saarimaki[43], R. Sadek[103], S. Sadhu[31], S. Sadovsky[140], J. Saetre[20], K. Šafařík[35], P. Saha[41], S. K. Saha[4], S. Saha[80], B. Sahoo[46], B. Sahoo[47], R. Sahoo[47], S. Sahoo[60], D. Sahu[47], P. K. Sahu[60], J. Saini[132], K. Sajdakova[37], S. Sakai[123], M. P. Salvan[97], S. Sambyal[91], I. Sanna[32,95], T. B. Saramela[110], D. Sarkar[134], N. Sarkar[132], P. Sarma[41], V. Sarritzu[22], V. M. Sarti[95], M. H. P. Sas[137], J. Schambach[87], H. S. Scheid[63], C. Schiaua[45], R. Schicker[94], A. Schmah[94], C. Schmidt[97], H. R. Schmidt[93], M. O. Schmidt[32], M. Schmidt[93], N. V. Schmidt[87], A. R. Schmier[120], R. Schotter[127], A. Schröter[38], J. Schukraft[32], K. Schwarz[97], K. Schweda[97], G. Scioli[25], E. Scomparin[55], J. E. Seger[14], Y. Sekiguchi[122], D. Sekihata[122], I. Selyuzhenkov[97,140], S. Senyukov[127], J. J. Seo[57], D. Serebryakov[140], L. Šerkšnytė[95], A. Sevcenco[62], T. J. Shaba[67], A. Shabetai[103], R. Shahoyan[32], A. Shangaraev[140], A. Sharma[90], B. Sharma[91], D. Sharma[46], H. Sharma[53,107], M. Sharma[91], S. Sharma[76], S. Sharma[91], U. Sharma[91], A. Shatat[72], O. Sheibani[114], K. Shigaki[92], M. Shimomura[77], J. Shin[11], S. Shirinkin[140], Q. Shou[39], Y. Sibiriak[140], S. Siddhanta[51], T. Siemiarczuk[79], T. F. Silva[110], D. Silvermyr[75], T. Simantathammakul[105], R. Simeonov[36], B. Singh[91], B. Singh[95], R. Singh[80], R. Singh[91], R. Singh[47], S. Singh[15], V. K. Singh[132], V. Singhal[132], T. Sinha[99], B. Sitar[12], M. Sitta[55,130], T. B. Skaali[19], G. Skorodumovs[94], M. Slupecki[43], N. Smirnov[137], R. J. M. Snellings[58], E. H. Solheim[19], J. Song[114], A. Songmoolnak[105], C. Sonnabend[32,97], F. Soramel[27], A. B. Soto-hernandez[88], R. Spijkers[84], I. Sputowska[107], J. Staa[75], J. Stachel[94], I. Stan[62], P. J. Steffanic[120], S. F. Stiefelmaier[94], D. Stocco[103], I. Storehaug[19], P. Stratmann[135], S. Strazzi[25], C. P. Stylianidis[84], A. A. P. Suaide[110], C. Suire[72], M. Sukhanov[140], M. Suljic[32], R. Sultanov[140], V. Sumberia[91], S. Sumowidagdo[82], S. Swain[60], I. Szarka[12], M. Szymkowski[133], S. F. Taghavi[95], G. Taillepied[97], J. Takahashi[111], G. J. Tambave[80], S. Tang[6,125], Z. Tang[118], J. D. Tapia Takaki[116], N. Tapus[124], L. A. Tarasovicova[135], M. G. Tarzila[45], G. F. Tassielli[31], A. Tauro[32], G. Tejeda Muñoz[44], A. Telesca[32], L. Terlizzi[24], C. Terrevoli[114], S. Thakur[4], D. Thomas[108], A. Tikhonov[140], A. R. Timmins[114], M. Tkacik[106], T. Tkacik[106], A. Toia[63], R. Tokumoto[92], N. Topilskaya[140], M. Toppi[48], F. Torales-Acosta[18], T. Tork[72], A. G. Torres Ramos[31], A. Trifiró[30,52], A. S. Triolo[30,32,52], S. Tripathy[50], T. Tripathy[46], S. Trogolo[32], V. Trubnikov[3], W. H. Trzaska[115], T. P. Trzcinski[133], A. Tumkin[140], R. Turrisi[53], T. S. Tveter[19], K. Ullaland[20], B. Ulukutlu[95], A. Uras[126], M. Urioni[54,131], G. L. Usai[22], M. Vala[37], N. Valle[21], L. V. R. van Doremalen[58], M. van Leeuwen[84], C. A. van Veen[94], R. J. G. van Weelden[84], P. Vande Vyvre[32], D. Varga[136], Z. Varga[136], M. Vasileiou[78], A. Vasiliev[140], O. Vázquez Doce[48], V. Vechernin[140], E. Vercellin[24], S. Vergara Limón[44], L. Vermunt[97], R. Vértesi[136], M. Verweij[58], L. Vickovic[33], Z. Vilakazi[121], O. Villalobos Baillie[100], A. Villani[23], G. Vino[49], A. Vinogradov[140], T. Virgili[28], M. M. O. Virta[115], V. Vislavicius[75], A. Vodopyanov[141], B. Volkel[32], M. A. Völkl[94], K. Voloshin[140], S. A. Voloshin[134], G. Volpe[31], B. von Haller[32], I. Vorobyev[95], N. Vozniuk[140], J. Vrláková[37], C. Wang[39], D. Wang[39], Y. Wang[39], A. Wegrzynek[32], F. T. Weiglhofer[38], S. C. Wenzel[32], J. P. Wessels[135], S. L. Weyhmiller[137], J. Wiechula[63], J. Wikne[19], G. Wilk[79], J. Wilkinson[97], G. A. Willems[135], B. Windelband[94], M. Winn[128], J. R. Wright[108], W. Wu[39], Y. Wu[118], R. Xu[6], A. Yadav[42], A. K. Yadav[132], S. Yalcin[71], Y. Yamaguchi[92], S. Yang[20], S. Yano[92], Z. Yin[6], I.-K. Yoo[16], J. H. Yoon[57], S. Yuan[20], A. Yuncu[94], V. Zaccolo[23], C. Zampolli[32], F. Zanone[94], N. Zardoshti[32], A. Zarochentsev[140], P. Závada[61], N. Zaviyalov[140], M. Zhalov[140], B. Zhang[6], L. Zhang[39], S. Zhang[39], X. Zhang[6], Y. Zhang[118], Z. Zhang[6], M. Zhao[10], V. Zherebchevskii[140], Y. Zhi[10], D. Zhou[6], Y. Zhou[83], J. Zhu[6,97], Y. Zhu[6], S. C. Zugravel[55], N. Zurlo[54,131]

[1] A.I. Alikhanyan National Science Laboratory (Yerevan Physics Institute) Foundation, Yerevan, Armenia

[2] AGH University of Science and Technology, Cracow, Poland
[3] Bogolyubov Institute for Theoretical Physics, National Academy of Sciences of Ukraine, Kiev, Ukraine
[4] Department of Physics, Centre for Astroparticle Physics and Space Science (CAPSS), Bose Institute, Kolkata, India
[5] California Polytechnic State University, San Luis Obispo, CA, USA
[6] Central China Normal University, Wuhan, China
[7] Centro de Aplicaciones Tecnológicas y Desarrollo Nuclear (CEADEN), Havana, Cuba
[8] Centro de Investigación y de Estudios Avanzados (CINVESTAV), Mexico City and Mérida, Mexico
[9] Chicago State University, Chicago, IL, USA
[10] China Institute of Atomic Energy, Beijing, China
[11] Chungbuk National University, Cheongju, Republic of Korea
[12] Faculty of Mathematics, Physics and Informatics, Comenius University Bratislava, Bratislava, Slovak Republic
[13] COMSATS University Islamabad, Islamabad, Pakistan
[14] Creighton University, Omaha, NE, USA
[15] Department of Physics, Aligarh Muslim University, Aligarh, India
[16] Department of Physics, Pusan National University, Pusan, Republic of Korea
[17] Department of Physics, Sejong University, Seoul, Republic of Korea
[18] Department of Physics, University of California, Berkeley, CA, USA
[19] Department of Physics, University of Oslo, Oslo, Norway
[20] Department of Physics and Technology, University of Bergen, Bergen, Norway
[21] Dipartimento di Fisica, Università di Pavia, Pavia, Italy
[22] Dipartimento di Fisica dell'Università and Sezione INFN, Cagliari, Italy
[23] Dipartimento di Fisica dell'Università and Sezione INFN, Trieste, Italy
[24] Dipartimento di Fisica dell'Università and Sezione INFN, Turin, Italy
[25] Dipartimento di Fisica e Astronomia dell'Università and Sezione INFN, Bologna, Italy
[26] Dipartimento di Fisica e Astronomia dell'Università and Sezione INFN, Catania, Italy
[27] Dipartimento di Fisica e Astronomia dell'Università and Sezione INFN, Padua, Italy
[28] Dipartimento di Fisica 'E.R. Caianiello' dell'Università and Gruppo Collegato INFN, Salerno, Italy
[29] Dipartimento DISAT del Politecnico and Sezione INFN, Turin, Italy
[30] Dipartimento di Scienze MIFT, Università di Messina, Messina, Italy
[31] Dipartimento Interateneo di Fisica 'M. Merlin' and Sezione INFN, Bari, Italy
[32] European Organization for Nuclear Research (CERN), Geneva, Switzerland
[33] Faculty of Electrical Engineering, Mechanical Engineering and Naval Architecture, University of Split, Split, Croatia
[34] Faculty of Engineering and Science, Western Norway University of Applied Sciences, Bergen, Norway
[35] Faculty of Nuclear Sciences and Physical Engineering, Czech Technical University in Prague, Prague, Czech Republic
[36] Faculty of Physics, Sofia University, Sofia, Bulgaria
[37] Faculty of Science, P.J. Šafárik University, Kosice, Slovak Republic
[38] Frankfurt Institute for Advanced Studies, Johann Wolfgang Goethe-Universität Frankfurt, Frankfurt, Germany
[39] Fudan University, Shanghai, China
[40] Gangneung-Wonju National University, Gangneung, Republic of Korea
[41] Department of Physics, Gauhati University, Guwahati, India
[42] Helmholtz-Institut für Strahlen- und Kernphysik, Rheinische Friedrich-Wilhelms-Universität Bonn, Bonn, Germany
[43] Helsinki Institute of Physics (HIP), Helsinki, Finland
[44] High Energy Physics Group, Universidad Autónoma de Puebla, Puebla, Mexico
[45] Horia Hulubei National Institute of Physics and Nuclear Engineering, Bucharest, Romania
[46] Indian Institute of Technology Bombay (IIT), Mumbai, India
[47] Indian Institute of Technology Indore, Indore, India
[48] INFN, Laboratori Nazionali di Frascati, Frascati, Italy
[49] INFN, Sezione di Bari, Bari, Italy
[50] INFN, Sezione di Bologna, Bologna, Italy
[51] INFN, Sezione di Cagliari, Cagliari, Italy
[52] INFN, Sezione di Catania, Catania, Italy
[53] INFN, Sezione di Padova, Padua, Italy
[54] INFN, Sezione di Pavia, Pavia, Italy

[55] INFN, Sezione di Torino, Turin, Italy
[56] INFN, Sezione di Trieste, Trieste, Italy
[57] Inha University, Incheon, Republic of Korea
[58] Institute for Gravitational and Subatomic Physics (GRASP), Utrecht University/Nikhef, Utrecht, The Netherlands
[59] Institute of Experimental Physics, Slovak Academy of Sciences, Kosice, Slovak Republic
[60] Institute of Physics, Homi Bhabha National Institute, Bhubaneswar, India
[61] Institute of Physics of the Czech Academy of Sciences, Prague, Czech Republic
[62] Institute of Space Science (ISS), Bucharest, Romania
[63] Institut für Kernphysik, Johann Wolfgang Goethe-Universität Frankfurt, Frankfurt, Germany
[64] Instituto de Ciencias Nucleares, Universidad Nacional Autónoma de México, Mexico City, Mexico
[65] Instituto de Física, Universidade Federal do Rio Grande do Sul (UFRGS), Porto Alegre, Brazil
[66] Instituto de Física, Universidad Nacional Autónoma de México, Mexico City, Mexico
[67] iThemba LABS, National Research Foundation, Somerset West, South Africa
[68] Jeonbuk National University, Jeonju, Republic of Korea
[69] Johann-Wolfgang-Goethe Universität Frankfurt Institut für Informatik, Fachbereich Informatik und Mathematik, Frankfurt, Germany
[70] Korea Institute of Science and Technology Information, Daejeon, Republic of Korea
[71] KTO Karatay University, Konya, Turkey
[72] Laboratoire de Physique des 2 Infinis, Irène Joliot-Curie, Orsay, France
[73] Laboratoire de Physique Subatomique et de Cosmologie, CNRS-IN2P3, Université Grenoble-Alpes, Grenoble, France
[74] Lawrence Berkeley National Laboratory, Berkeley, CA, USA
[75] Division of Particle Physics, Department of Physics, Lund University, Lund, Sweden
[76] Nagasaki Institute of Applied Science, Nagasaki, Japan
[77] Nara Women's University (NWU), Nara, Japan
[78] Department of Physics, School of Science, National and Kapodistrian University of Athens, Athens, Greece
[79] National Centre for Nuclear Research, Warsaw, Poland
[80] National Institute of Science Education and Research, Homi Bhabha National Institute, Jatni, India
[81] National Nuclear Research Center, Baku, Azerbaijan
[82] National Research and Innovation Agency-BRIN, Jakarta, Indonesia
[83] Niels Bohr Institute, University of Copenhagen, Copenhagen, Denmark
[84] Nikhef, National Institute for Subatomic Physics, Amsterdam, The Netherlands
[85] Nuclear Physics Group, STFC Daresbury Laboratory, Daresbury, UK
[86] Nuclear Physics Institute of the Czech Academy of Sciences, Husinec-Řež, Czech Republic
[87] Oak Ridge National Laboratory, Oak Ridge, TN, USA
[88] Ohio State University, Columbus, OH, USA
[89] Physics Department, Faculty of science, University of Zagreb, Zagreb, Croatia
[90] Physics Department, Panjab University, Chandigarh, India
[91] Physics Department, University of Jammu, Jammu, India
[92] Physics Program and International Institute for Sustainability with Knotted Chiral Meta Matter (SKCM2), Hiroshima University, Hiroshima, Japan
[93] Physikalisches Institut, Eberhard-Karls-Universität Tübingen, Tübingen, Germany
[94] Physikalisches Institut, Ruprecht-Karls-Universität Heidelberg, Heidelberg, Germany
[95] Physik Department, Technische Universität München, Munich, Germany
[96] Politecnico di Bari and Sezione INFN, Bari, Italy
[97] Research Division and ExtreMe Matter Institute EMMI, GSI Helmholtzzentrum für Schwerionenforschung GmbH, Darmstadt, Germany
[98] Saga University, Saga, Japan
[99] Saha Institute of Nuclear Physics, Homi Bhabha National Institute, Kolkata, India
[100] School of Physics and Astronomy, University of Birmingham, Birmingham, UK
[101] Sección Física, Departamento de Ciencias, Pontificia Universidad Católica del Perú, Lima, Peru
[102] Stefan Meyer Institut für Subatomare Physik (SMI), Vienna, Austria
[103] SUBATECH, IMT Atlantique, CNRS-IN2P3, Nantes Université, Nantes, France
[104] Sungkyunkwan University, Suwon City, Republic of Korea

[105] Suranaree University of Technology, Nakhon Ratchasima, Thailand
[106] Technical University of Košice, Kosice, Slovak Republic
[107] The Henryk Niewodniczanski Institute of Nuclear Physics, Polish Academy of Sciences, Cracow, Poland
[108] The University of Texas at Austin, Austin, TX, USA
[109] Universidad Autónoma de Sinaloa, Culiacán, Mexico
[110] Universidade de São Paulo (USP), São Paulo, Brazil
[111] Universidade Estadual de Campinas (UNICAMP), Campinas, Brazil
[112] Universidade Federal do ABC, Santo Andre, Brazil
[113] University of Cape Town, Cape Town, South Africa
[114] University of Houston, Houston, TX, USA
[115] University of Jyväskylä, Jyvaskyla, Finland
[116] University of Kansas, Lawrence, KS, USA
[117] University of Liverpool, Liverpool, UK
[118] University of Science and Technology of China, Hefei, China
[119] University of South-Eastern Norway, Kongsberg, Norway
[120] University of Tennessee, Knoxville, TN, USA
[121] University of the Witwatersrand, Johannesburg, South Africa
[122] University of Tokyo, Tokyo, Japan
[123] University of Tsukuba, Tsukuba, Japan
[124] University Politehnica of Bucharest, Bucharest, Romania
[125] CNRS/IN2P3, LPC, Université Clermont Auvergne, Clermont-Ferrand, France
[126] CNRS/IN2P3, Institut de Physique des 2 Infinis de Lyon, Université de Lyon, Lyon, France
[127] CNRS, IPHC UMR 7178, Université de Strasbourg, 67000 Strasbourg, France
[128] Départment de Physique Nucléaire (DPhN), IRFU, Université Paris-Saclay Centre d'Etudes de Saclay (CEA), Saclay, France
[129] Università degli Studi di Foggia, Foggia, Italy
[130] Università del Piemonte Orientale, Vercelli, Italy
[131] Università di Brescia, Brescia, Italy
[132] Variable Energy Cyclotron Centre, Homi Bhabha National Institute, Kolkata, India
[133] Warsaw University of Technology, Warsaw, Poland
[134] Wayne State University, Detroit, MI, USA
[135] Institut für Kernphysik, Westfälische Wilhelms-Universität Münster, Münster, Germany
[136] Wigner Research Centre for Physics, Budapest, Hungary
[137] Yale University, New Haven, CT, USA
[138] Yonsei University, Seoul, Republic of Korea
[139] Zentrum für Technologie und Transfer (ZTT), Worms, Germany
[140] Affiliated with an Institute Covered by a Cooperation Agreement with CERN, Geneva, Switzerland
[141] Affiliated with an International Laboratory Covered by a Cooperation Agreement with CERN, Geneva, Switzerland

[a] Also at: Max-Planck-Institut für Physik, Munich, Germany
[b] Also at: Italian National Agency for New Technologies, Energy and Sustainable Economic Development (ENEA), Bologna, Italy
[c] Also at: Department of Applied Physics, Aligarh Muslim University, Aligarh, India
[d] Also at: Institute of Theoretical Physics, University of Wroclaw, Wrocław, Poland
[e] Also at: An Institution Covered by a Cooperation Agreement with CERN, Geneva, Switzerland
[f] Deceased